

## Electroadhesion with application to touchscreens

Omer Sirin, Mehmet Ayyildiz, Bo Persson, Cagatay Basdogan

► **To cite this version:**

Omer Sirin, Mehmet Ayyildiz, Bo Persson, Cagatay Basdogan. Electroadhesion with application to touchscreens. *Soft Matter*, Royal Society of Chemistry, 2019, 15 (8), pp.1758-1775. 10.1039/C8SM02420K . hal-03176831

**HAL Id: hal-03176831**

**<https://hal.archives-ouvertes.fr/hal-03176831>**

Submitted on 22 Mar 2021

**HAL** is a multi-disciplinary open access archive for the deposit and dissemination of scientific research documents, whether they are published or not. The documents may come from teaching and research institutions in France or abroad, or from public or private research centers.

L'archive ouverte pluridisciplinaire **HAL**, est destinée au dépôt et à la diffusion de documents scientifiques de niveau recherche, publiés ou non, émanant des établissements d'enseignement et de recherche français ou étrangers, des laboratoires publics ou privés.

Cite this: DOI: 10.1039/xxxxxxxxxx

## Electroadhesion with application to touchscreens

Omer Sirin,<sup>a</sup> Mehmet Ayyildiz,<sup>bc</sup> Bo Persson,<sup>bd</sup> and Cagatay Basdogan<sup>a</sup>Received Date  
Accepted Date

DOI: 10.1039/xxxxxxxxxx

www.rsc.org/journalname

There is a growing interest on touchscreens displaying tactile feedback due to their tremendous potential in consumer electronics. In these systems, the friction between user's fingerpad and the surface of touchscreen is modulated to display tactile effects. One of the promising techniques used in this regard is electrostatic actuation. If, for example, an alternating voltage is applied to the conductive layer of a surface capacitive touchscreen, an attractive electrostatic force is generated between finger and the surface which results in an increase in frictional forces acting on the finger moving on the surface. By altering the amplitude, frequency, and the waveform of this signal, a rich set of tactile effects can be generated on the touchscreen. Despite the ease of implementation and its powerful effect on our tactile sensation, the contact mechanics leading to an increase in friction due to electroadhesion has not been fully understood yet. In this paper, we present experimental results for how the friction between a finger and a touchscreen depends on the electrostatic attraction and the applied normal pressure. The dependency of the finger–touchscreen interaction on the applied voltage, and on several other parameters, is also investigated using a mean field theory based on multiscale contact mechanics. We present detailed theoretical analysis of how the area of real contact and the friction force depend on contact parameters, and show that it is possible to further augment the friction force, and hence the tactile feedback displayed to the user by carefully choosing those parameters.

### 1 Introduction

Touchscreen, a display screen that is sensitive to the touch of a finger or stylus, has been available for nearly half a century. It has been widely used on ATM machines, retail point-of-sale terminals, game consoles, car navigation systems, medical monitors, and industrial control panels. After the introduction of touchscreen-based mobile devices in the late 2000s, the capacitive touchscreen has become widely popular on handheld devices such as personal computers, tablets, personal digital assistants, smart watches, and e-book readers. Today, the touchscreen is one of the easiest to use and most intuitive of all computer interfaces, which allows users to naturally and directly interact with what is displayed (text, pictures and other data), rather than using a traditional keyboard or mouse. One important effort to make this interaction more powerful is to provide effective, feasible and inexpensive tactile feedback to the user. In this regard, two leading surface haptic technologies have emerged during the last few years. One is based on the modulation of friction between human fingertip and active surface through electroadhesion.<sup>1–5</sup> Another involves ul-

trasonic vibrations to reduce the friction, and generate a squeeze film effect (creating a thin cushion of air) between the fingertip and the counter surface.<sup>6,7</sup>

The electrical attraction between a charged surface and human skin was discovered by Johnsen and Rahbek<sup>8</sup> in 1923. Later, in 1953 Mallinckrodt<sup>9</sup> reported an increase in the friction during touch when an alternating voltage is applied to an insulated aluminum plate. He observed that the input voltage signal creates an alternating electrostatic force that periodically attracts and releases the finger from the surface, producing a friction-like rubbery sensations when the finger moves on the surface. This effect is now intensively studied, e.g., for grippers for robotics,<sup>10–12</sup> and in the context of mobile touchscreens.<sup>13,14</sup> In particular, the potential applications of touchscreens displaying tactile feedback in education, games, communication, data visualization, and user interface development for blinded people are highly promising.

When an alternating electric potential is applied to the conductive layer of a touchscreen, the insulating layer on the glass plate and the finger are polarized by induction (i.e., charges of opposite sign are accumulated on the surfaces at the contacting interface). Thus, an electrostatic attraction force due to “electroadhesion”, is generated between the finger and the counter surface in the normal direction; which increases the sliding friction between the finger and the glass plate. This phenomenon was referred to as “electrovibration” by Grimnes,<sup>15</sup> who also reported that the gen-

<sup>a</sup> College of Engineering, Koc University, Istanbul, Turkey<sup>b</sup> PGI-1, FZ Jülich, Germany, EU<sup>c</sup> Faculty of Engineering and Natural Sciences, Istanbul Bilgi University, Istanbul, Turkey<sup>d</sup> www.MultiscaleConsulting.com

erated tactile sensation depends on the roughness and moisture of the finger.

The human skin is highly sensitive to variations in friction force. The nature of the contact interface and involved materials (e.g., surface topographies, contamination films, and the atomic and molecular characteristics) strongly influence the sliding friction,<sup>16–18</sup> in addition to the external conditions such as temperature, humidity, mechanical vibrations and electric fields. For example, the friction force generated by the electrostatic attraction depends on the frequency, waveform and the amplitude of the applied electric potential.<sup>2,5,19</sup> A rich set of tactile effects can be potentially generated by varying these parameters.<sup>4</sup> In spite of the ease of implementation and its powerful effect on our tactile sensation, the contact mechanics leading to an increase in friction due to electroadhesion has not been fully understood yet.

In this paper, we present theoretical and experimental results for the estimation of the friction resulting from the electrostatic attraction between the human finger and a touchscreen. The dependency of the finger–touchscreen interaction on the applied voltage, and on several other contact parameters, was investigated using a mean field theory based on multiscale contact mechanics. For the experimental measurements, a tribometer was developed to move the index finger of an experimenter back and forth on the touchscreen using a motorized slider. The friction force at the sliding speed of  $v = 50$  mm/s was recorded as a function of the normal force, varied incrementally 0.2 N and 2 N. The amplitude of the voltage signal applied to the conductive layer of the touchscreen at 125 Hz was varied between  $V_0 = 0$  V to  $V_0 = 200$  V (with an increment of 25 V). The experimental results were compared to those produced by the theory. Also, the dependency of the electroadhesion friction on the frequency of the oscillating electric potential was investigated using the proposed theory. Finally, a discussion on the origin and enhancement of the friction due to electroadhesion is provided, along with the corresponding design criteria; and also the limitations of the study and the challenges ahead are discussed.

## 2 Theory: Mean field model for electroadhesion

Fig. 1 shows an elastic solid having a multi-scale surface roughness above a rigid solid having a flat and smooth surface. Both solids are conducting materials with insulating surface layers of thickness  $d_1$  and  $d_2$ , and dielectric constants  $\epsilon_1$  and  $\epsilon_2$ . We define the effective insulator thickness as  $h_0 = d_1/\epsilon_1 + d_2/\epsilon_2$ . The interfacial separation  $u = u(\mathbf{x})$  between the solids depends on the lateral coordinate  $\mathbf{x} = (x, y)$ .

The solids make atomic contact in a fraction  $A/A_0$  of the nominal contact area  $A_0$  (in the figure  $A = 0$ ). The non-contact regions are filled with air but we can consider these regions as vacuum because of the (relative) dielectric constant of air ( $\epsilon_{\text{air}} \approx 1.00059$ ) is nearly the same as of vacuum ( $\epsilon = 1$ ).

Assume now that an electric potential  $\phi(t) = V_0 \cos(\omega_0 t)$  is applied between the solids as indicated in Fig. 1. This will give rise to an electric field in the air-gap between the solids, which results in an attractive force that can be calculated from the  $zz$ -

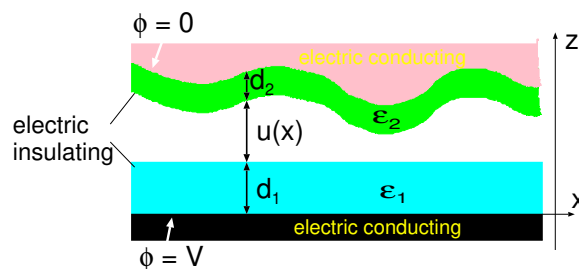


**Fig. 1** An elastic solid with surface roughness above a rigid solid with a flat surface. Both solids are conducting materials with insulating surface layers of thickness  $d_1$  and  $d_2$  and dielectric constants  $\epsilon_1$  and  $\epsilon_2$ . An electric voltage difference  $V$  occurs between the two conducting solids. The interfacial separation  $u = u(\mathbf{x})$  depends on the lateral coordinate  $\mathbf{x} = (x, y)$ .

component of the Maxwell stress tensor:<sup>20</sup>

$$\sigma_{zz} = \frac{1}{2} \epsilon_0 E_z^2, \quad (1)$$

where  $\epsilon_0$  is the dielectric function of vacuum. The electric field at bottom surface of the upper solid (the SC-air interface) is:<sup>20</sup>

$$E_z = -\text{Re} \left[ \frac{V_0 e^{-i\omega_0 t}}{u + h_0(\omega)} \right]. \quad (2)$$

The normal stress averaged over the surface roughness becomes

$$\langle \sigma_{zz} \rangle = \frac{1}{4} \epsilon_0 V_0^2 \int_0^\infty du P(p, u) \frac{1 + \cos(2\omega_0 t + 2\phi)}{|u + h_0(\omega_0)|^2}, \quad (3)$$

where  $P(p, u)$  is the probability distribution for the interfacial separation  $u$ , which depends on the squeezing pressure  $p$  (see below).

Assume that we squeeze the upper solid against the substrate with a force  $F_0$ . When an electric potential is applied between the solids, there will be an additional electric force acting on them. In the simplest approach, one includes the electric attraction  $p_a = \langle \sigma_{zz} \rangle$  as a contribution to the external load. Thus we write the effective squeezing or loading pressure as

$$p = p_0 + p_a, \quad (4)$$

where  $p_0 = F_0/A_0$  is the applied pressure. Intuitively, one expects this approach to be accurate when the interaction force between the surfaces is long-range. A similar approach has been also successfully used for modeling the attraction resulting from capillary bridges.<sup>21,22</sup>

To calculate  $p_a = \langle \sigma_{zz} \rangle$ , we need to know the probability distribution  $P(p, u)$ . For randomly rough surfaces, the function  $P(p, u)$  has been approximately calculated.<sup>23,24</sup> Using eqn (3) and (4), the time (and space) average of the effective pressure is obtained as

$$p = p_0 + \frac{1}{4} \epsilon_0 V_0^2 \int_0^\infty du P(p, u) \frac{1}{|u + h_0|^2}. \quad (5)$$

The electric potential can be calculated from the above equation as

$$V_0^2 = \frac{4(p - p_0)/\epsilon_0}{\int_0^\infty du P(p, u) |u + h_0|^{-2}}. \quad (6)$$

For a homogeneous elastic solid, the relative contact area  $A/A_0$  can be obtained by using<sup>25</sup>

$$\frac{A}{A_0} \approx \frac{\sqrt{\pi}}{2} \operatorname{erf} \left( \frac{2p}{h'E^*} \right), \quad (7)$$

where  $h'$  is the rms slope of the combined surface roughness profile and  $E^* = E/(1 - \nu^2)$  (where  $E$  and  $\nu$  are the Young's modulus and Poisson ratio of the elastic solid, respectively). This equation is valid for the contact between homogeneous elastic solids with random surface roughness. When  $A/A_0 \ll 1$ , eqn (7) reduces to

$$\frac{A}{A_0} \approx \frac{2p}{h'E^*}. \quad (8)$$

The human skin is a layered material and hence  $h'$  is not the rms-slope of the combined surface roughness, but a quantity which depends on the surface roughness power spectrum as well as the elastic modulus and thickness of the layers.<sup>26</sup> In addition, for dry skin, the local contact pressures are typically so large that plastic deformation may occur, and in this case one cannot use eqn (7) or (8) directly to calculate the contact area but the full theory described elsewhere<sup>25,26</sup> must be used.

From the knowledge of  $A$ , we obtain the friction force from

$$F_f = A\tau_f. \quad (9)$$

The frictional shear stress  $\tau_f$  is independent of the asperity contact pressure  $p^* = pA_0/A$  as long as  $p^*$  is less than a few MPa. As an example, which is of interest for grippers in robotics applications, for silicone rubber (PDMS) sliding (in complete contact) on a smooth glass surface with a speed of  $v \approx 1$  mm/s, the experiments have shown that  $\tau_f \approx 0.1$  MPa.<sup>27</sup> At the same sliding speed, for other types of rubber  $\tau_f \approx 1 - 10$  MPa,<sup>28,29</sup> and for the human skin, which is of interest for touchscreens,  $\tau_f = 5 - 13$  MPa.<sup>30,31</sup> This is also similar to what is observed for plastics (polymers below the glass transition temperature).<sup>32</sup>

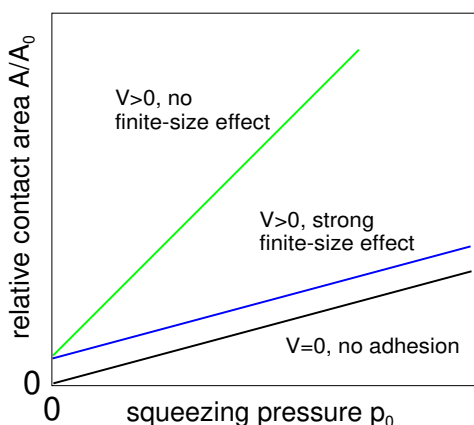


**Fig. 2** The relative contact area as a function of the squeezing pressure without adhesion (black line), with adhesion for a system with negligible finite-size effect (green line), and for a system with a strong finite-size effect (blue line). (Schematic).

We note that electroadhesion for the dry finger skin depends on what is called as finite size effect (see Appendix A), and that adhe-

sion exists even if the solids are rigid. When finite size effects are important, one expects the contact area  $A$  to depend on the nominal contact pressure  $p_0$  (for small contact pressures) as shown in Fig. 2 (blue curve). Note that, the contact area curve  $A(p_0)$  with adhesion when finite size effects are important (blue curve) is nearly parallel with the one without the adhesion (black curve). This differs drastically from the case where finite size effects are negligible and the change in the contact area as a function of load (for small applied load) has the form shown with the green line in Fig. 2. In this case, the slope of the  $A(p_0)$  line is much bigger than when finite size effects are important. Our experiments and the theoretical analysis show that finite size effects can be important for the dry finger skin having high elastic modulus of the SC,  $E_{SC}$ .

## 2.1 Comparison with earlier studies

Let us compare our basic formula for the electroadhesion pressure with what have been used before. First, using eqn (3) and the definition of effective insulator layer thickness, we obtain;

$$p_a = \frac{1}{4} \epsilon_0 V_0^2 \int_0^\infty du P(p, u) \frac{1 + \cos(2\omega_0 t + \phi)}{|u + d_1/\epsilon_1 + d_2/\epsilon_2|^2}. \quad (10)$$

If we assume that the air-film has a *uniform* thickness  $\bar{u}$ , then the probability distribution becomes  $P(p, u) = \delta(u - \bar{u})$  and the time average of eqn (10) takes the form

$$p_a = \frac{1}{4} \frac{\epsilon_0 V_0^2}{|\bar{u} + d_1/\epsilon_1 + d_2/\epsilon_2|^2}. \quad (11)$$

If we also assume that the dielectric functions  $\epsilon_1(\omega_0)$  and  $\epsilon_2(\omega_0)$  are real, then we get

$$p_a = \frac{1}{4} \frac{\epsilon_0 V_0^2}{(\bar{u} + d_1/\epsilon_1 + d_2/\epsilon_2)^2}. \quad (12)$$

This equation has been used in earlier studies to calculate the electroadhesive force per unit surface area.<sup>33</sup> However, it would be valid only if (a) the air film would have uniform thickness  $\bar{u}$ , and (b) the dielectric functions of the SC and the insulating layer would be real. The assumption (b) is a reasonable one in most cases of interest, but the assumption (a) is a poor one when the average thickness of the air gap (determined mainly by the surface roughness of the SC)  $\bar{u} \approx 10 \mu\text{m}$  is much larger than the effective thickness  $h_0 = d_1/\epsilon_1 + d_2/\epsilon_2 \approx 0.3 \mu\text{m}$ . The reason for this is that in the expression (10) the most important contribution arises when  $u$  is small, i.e., from the areas of real contacts, and from the so called rim-areas which are narrow strips of non-contact areas around the contact regions where the surface separation  $u(\mathbf{x})$  is very small.

The assumption (b) breaks down when the electrical conductivity of the SC (or of the insulating glass film) becomes important, which is the case at very low frequency  $\omega$ . For low frequencies, the dielectric function of the SC is of the form

$$\epsilon = \epsilon_{SC} + \frac{i}{\omega \epsilon_0 \rho_{SC}}, \quad (13)$$

where  $\rho_{SC}(\omega)$  is the (frequency-dependent) electrical resistivity of the skin SC (see Fig. 7). Note that when  $1/(\omega \epsilon_0 \rho_{SC}) > \epsilon_{SC}$

or  $\omega < 1/(\epsilon_0 \epsilon_{SC} \rho_{SC})$ , the SC will act like a conducting layer, and the mobile charges in the skin will be located at the skin surface rather than at the interface between the SC and the underlying tissue of the skin. Measurements<sup>34</sup> for the dry human skin have shown that both  $\epsilon_{SC}$  and  $\rho_{SC}$  depend on the frequency and that  $1/(\omega \epsilon_0 \rho_{SC}) > \epsilon_{SC}$  for  $\omega < 200 \text{ s}^{-1}$  or 30 Hz (at this frequency Fig. 7 shows that  $\epsilon_{SC} \approx 5000$  and  $\rho_{SC} \approx 6 \times 10^4 \text{ } \Omega\text{m}$ ).

The area of real (atomic) contact between two solids depends on the resolution of the instrument used to measure it and decreases with increasing resolution (i.e., increasing magnification or decreasing pixel size). But, it also depends on the surface roughness so one cannot compare different cases directly without knowing the surface roughness (and effective elastic modulus). For the human fingertip squeezed against a smooth counter-surface, many studies<sup>35,36</sup> have been presented where it appears that the contact area is  $\sim 50\%$  of the nominal contact area. In our opinion, the area of atomic contact between dry skin and a flat counter surface is much smaller. Thus, neglecting the adhesion, the contact area may be of order  $2p_0/(E^*h')$ , where (typically) the squeezing pressure  $p_0 \approx 10 \text{ kPa}$ , the effective modulus  $E^* \approx 40 \text{ MPa}$ , and rms slope (from surface topography measurements)  $h' \approx 1$ , giving  $A/A_0 \approx 5 \times 10^{-4}$  or 0.05% relative contact. We attribute this difference between experimental observations and the theory to the limited resolution in experimental measurements and/or existence of liquid in the contact region (sweat or oil), which makes the fluid filled interfacial region appear as real contact!

For example, Fig. 3 shows an optical picture of a glass surface where the oil-water fluid film left on the surface from a few seconds contact with the index finger. The fluid covers more than 50% of the apparent contact area. However, most of the friction between the finger and the glass surface is derived from the region of real skin-glass contact, or where the fluid film thickness is very thin (in the order of a few nanometer or less).

## 2.2 Charge drift through the SC

We have argued above that if the frequency  $\omega$  is small enough, the finite conductivity of the SC will result in transfer of mobile charges to the SC-air and SC-glass interfaces. Here we study this problem in more detail for the case where the electric potential  $\phi(t)$  is turned-on in a step-like manner at time  $t = 0$ , see Fig. 4.

We define

$$\phi(\omega) = \frac{1}{2\pi} \int_{-\infty}^{\infty} dt \phi(t) e^{i\omega t}, \quad (14)$$

$$\phi(t) = \int_{-\infty}^{\infty} d\omega \phi(\omega) e^{-i\omega t}. \quad (15)$$

For the step function

$$\phi(\omega) = \frac{1}{2\pi} \int_0^{\infty} dt V_0 e^{-\epsilon t} e^{i\omega t} = \frac{1}{2\pi i} \frac{V_0}{\omega + i\epsilon}, \quad (16)$$

where we have included the factor  $\exp(-\epsilon t)$ , with  $\epsilon = 0^+$  an infinitesimal positive number, in order to make the integral well defined. The electric field becomes

$$E_z = \int_{-\infty}^{\infty} d\omega \frac{-\phi(\omega)}{u + h_0(\omega)} e^{-i\omega t},$$

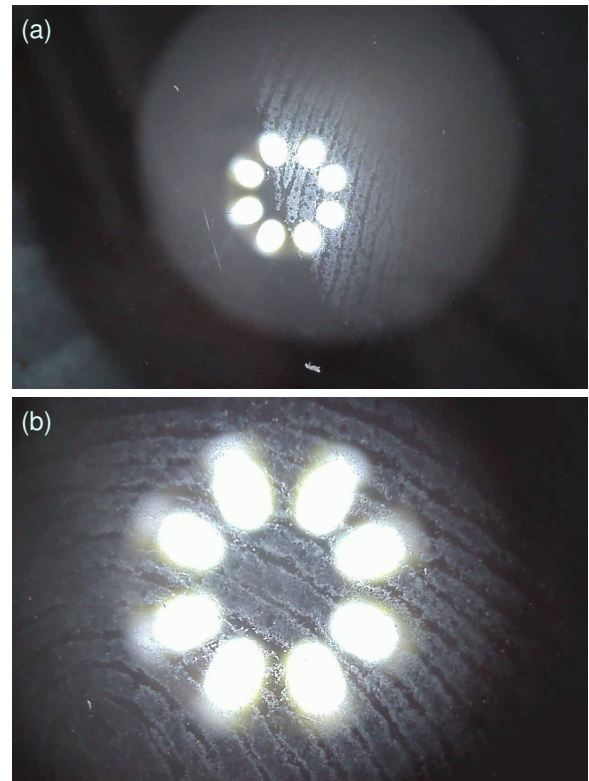


**Fig. 3** Optical microscope pictures at low (a) and high (b) magnification of the fluid left on a glass surface after contact with the index finger. The fluid is mainly oil as it does not evaporate even after long waiting time. If the finger is cleaned with soap and water, mainly water is deposited on the glass surface which disappears a few seconds after removing the finger due to evaporation. The white elliptical regions are reflections in the glass surface of 8 light diodes.

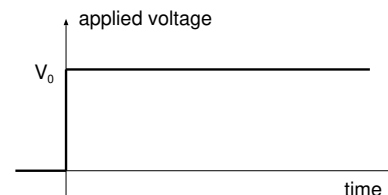


**Fig. 4** A step-like change in the electric potential  $\phi(t)$ , where  $\phi(t) = 0$  for  $t < 0$  and  $\phi(t) = V_0$  for  $t > 0$ .

$$= -\frac{1}{2\pi i} \int_{-\infty}^{\infty} d\omega V_0 \frac{1}{(u + h_0(\omega))(\omega + i\epsilon)} e^{-i\omega t} \quad (17)$$

Assuming that the dielectric function of the SC is of the form (13) with  $\epsilon_{SC}$  and  $\rho_{SC}$  constants, we can write

$$\frac{1}{u + h_0(\omega)} = \frac{a\omega + ib}{\omega + i\gamma}, \quad (18)$$

where

$$\begin{aligned} a &= \frac{1}{u + d_1/\epsilon_1 + d_2/\epsilon_{SC}}, \\ b &= \frac{a}{\epsilon_0 \rho_{SC} \epsilon_{SC}}, \\ \gamma &= b(u + d_1/\epsilon_1). \end{aligned} \quad (19)$$



We get

$$E_z = -\frac{V_0}{2\pi i} \int d\omega \frac{a\omega + ib}{\omega + i\gamma} \frac{1}{\omega + i\epsilon} e^{-i\omega t} \quad (20)$$

We can calculate this integral by closing the integration path in the complex  $\omega$ -space. This gives for  $t > 0$ :

$$E_z = V_0 \left[ \frac{b}{\gamma} + \left( a - \frac{b}{\gamma} \right) e^{-\gamma t} \right], \quad (21)$$

where

$$\frac{b}{\gamma} = \frac{1}{u + d_1/\epsilon_1}. \quad (22)$$

For  $t = 0$ , we get from (21):

$$E_z = \frac{V_0}{u + d_1/\epsilon_1 + d_2/\epsilon_{SC}}, \quad (23)$$

which corresponds to all the mobile charges located at the inner surface of the SC. For times  $t \gg \tau$ , where  $\tau = 1/\gamma$ , we have instead

$$E_z = \frac{V_0}{u + d_1/\epsilon_1}, \quad (24)$$

which is the expected result when all the mobile charges are on the SC-air interface. Hence, the relaxation time

$$\tau = \epsilon_0 \rho_{SC} \epsilon_{SC} \left( 1 + \frac{d_2/\epsilon_{SC}}{u + d_1/\epsilon_1} \right), \quad (25)$$

describes the time it takes for the mobile charges to move from the inner surface of the SC to the outer surface at the air interface. In reality, the glass substrate may have a finite electric surface conductivity, and a fraction of the mobile charges may leave the SC and distribute themselves on the glass surface. This would result in a reduction of the electric attraction between the finger and the skin.

One interesting experiment would be to measure the friction force as a function of time after applying the voltage at time  $t = 0$ . This would contain information about the charge transfer from the inner to the outer surface of the SC and maybe even to the glass surface. We also note that if there is a fluid with ions, e.g., sweat due to finger (moisture), in the nominal contact region, the electric potential in the gap between the finger and the counter-surface is influenced.

## 3 Materials and Methods

### 3.1 Skin model

The human skin is very complex material with non-homogeneous and non-linear viscoelastic properties. Here, we will use a simplified description which we believe is sufficient for modeling contact interactions with touchscreen under electroadhesion.

#### 3.1.1 Surface roughness

The surface topography of the (dry and wet) human wrist skin was already investigated by using optical and Atomic Force Microscopy.<sup>30,31</sup> From the measured topography, the surface roughness power spectrum was obtained. The red curve in Fig. 5 shows the surface roughness power spectrum of undeformed dry wrist skin as a function of the wavenumber (log-log scale). The surface has the rms roughness amplitude of 22  $\mu\text{m}$  and the rms slope

of 0.91. The linear region for  $q > 4 \times 10^5 \text{ m}^{-1}$  corresponds to a Hurst exponent  $H = 0.86$ . Using the roughness power spectrum of wrist skin as a reference, power spectrum curves for finger skin are constructed for different values of  $E_{SC}$ . The green and blue curves are the power spectrums of plastically deformed finger skin surfaces (obtained as described in Appendix A) assuming that Young's modulus of the stratum corneum is  $E_{SC} = 100 \text{ MPa}$  and  $E_{SC} = 1 \text{ GPa}$ , respectively, and the penetration hardness is  $\sigma_Y = 50 \text{ MPa}$ . For  $E_{SC} = 10 \text{ MPa}$  and  $E_{SC} = 1 \text{ MPa}$ , no plastic deformation occurs and in those cases we have used the power spectrum given by the red curve in Fig. 5. Some calculations given below are performed either with 4 times higher or 4 times smaller power spectrum in magnitude. These surfaces have the rms roughness amplitudes of 44  $\mu\text{m}$  and 11  $\mu\text{m}$ , respectively.

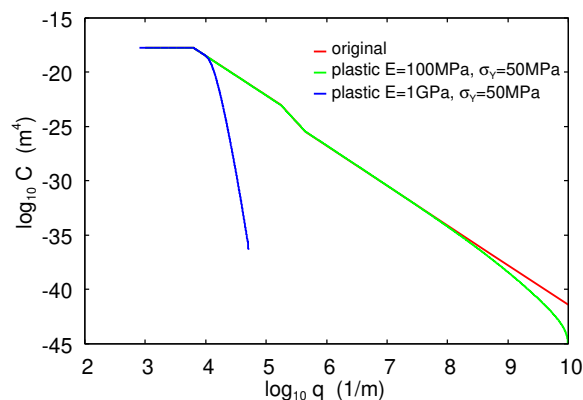


**Fig. 5** The surface roughness power spectrum as a function of the wavenumber (log-log scale). The power spectrum of the undeformed surface (red line) has the rms roughness amplitude 22  $\mu\text{m}$  and the rms slope 0.91. The linear region for  $q > 4 \times 10^5 \text{ m}^{-1}$  corresponds to a Hurst exponent  $H = 0.86$ . The green and blue lines are the power spectrums of the plastically deformed surfaces assuming  $E_{SC} = 100 \text{ MPa}$  and  $E_{SC} = 1 \text{ GPa}$ , respectively, and the penetration hardness of 50 MPa. For the plastic deformation calculations, we assume the thickness of the SC is 200  $\mu\text{m}$  and the elastic modulus of the tissue under the SC is  $E_{\text{bulk}} = 10 \text{ kPa}$ . The plastically smoothed surface profiles have the rms roughness of 22  $\mu\text{m}$  (green curve) and 20  $\mu\text{m}$  (blue curve).

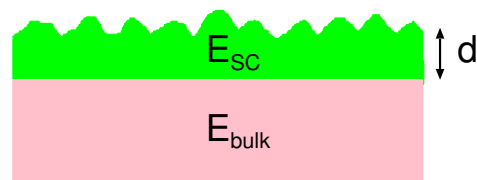


**Fig. 6** The model of the skin used in the theoretical calculations. The bulk elastic modulus is  $E_{\text{bulk}} = 10 - 30 \text{ kPa}$  and Poisson ratio is  $\nu_{\text{bulk}} = 0.5$ . The top layer (stratum corneum) is  $d = 100 - 200 \mu\text{m}$  thick and has the Young's modulus of  $E_{SC} \approx 1 - 10 \text{ MPa}$  in the wet state and  $E_{SC} \approx 0.1 - 1 \text{ GPa}$  in the dry state and the Poisson ratio is  $\nu_{SC} = 0.5$ .

#### 3.1.2 Mechanical properties

We treat the skin using a two layer model shown in Fig. 6. The bulk has a Young's elastic modulus denoted by  $E_{\text{bulk}}$  and Poisson ratio  $\nu_{\text{bulk}} = 0.5$ . The top layer [stratum corneum (SC)] has the thickness  $d_2$ , the Young's modulus  $E_{SC}$  and the Poisson ratio

$v_{SC} = 0.5$ . Since the thickness of the top layer and its elastic modulus can vary largely from one individual to another,<sup>37</sup> we have considered a range of parameters in our modeling calculations, namely

- (a)  $E_{SC} = 1, 10, 100, 1000$  MPa
- (b)  $d_2 = 100, 200, 300, 400$   $\mu\text{m}$
- (c)  $E_{\text{bulk}} = 3, 10, 30$  kPa

The large variation in  $E_{SC}$  is considered in this study to reflect the strong dependency of the elastic modulus of the SC on the humidity:  $E_{SC}$  decreases from  $\approx 1$  GPa in the dry state to 10 MPa (or less) in the wet state.<sup>38–41</sup> In the dry state, when the skin is squeezed against a hard counter surface, the contact pressure becomes so high that plastic deformation of the SC occurs in the asperity contact regions. In the study below, we take this into account by setting the penetration hardness to  $\sigma_Y = 50$  MPa.<sup>30,31,42</sup> We note that the plastic deformation of the SC is unlikely to involve breaking of strong covalent bonds, but rather involves moving segments of polymers over energetic barriers which are too high to be rapidly overcome by thermal fluctuations in the dry state. However, if the plastically deformed SC is exposed to high enough humidity, it swells, and the energetic barriers for segmental motion are reduced. In that case, the thermal motion can rearrange the polymer chains so that the SC takes its original undeformed state on return to the dry state. This situation is very similar to the behavior of rubber when plastically deformed at low temperatures.<sup>43</sup> The elastoplastic linear model we use for the SC is relatively simple. A better, but more complex description, would be a nonlinear viscoelastic model.

### 3.1.3 Electrical properties

The dielectric properties of the human skin has been measured by Yamamoto *et al.*<sup>34</sup>. In Fig. 7, we show the variation in dielectric constant and the electrical resistivity as a function of the stimulation frequency. In the frequency range of interest, from  $f = 0$  (static) to  $f = 1000$  Hz,  $\epsilon_{SC}$  decreases from  $\approx 10^4$  to  $\approx 10^3$ . The dielectric function (and electrical conductivity) of the bulk tissue under the SC is higher than that of the SC and will be considered as perfectly conducting in our analysis.

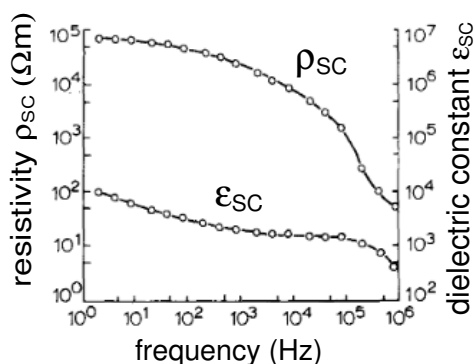


**Fig. 7** The dielectric constant and the resistivity of the human SC as a function of the stimulation frequency (adopted from Yamamoto *et al.*<sup>34</sup>).

### 3.2 Touchscreen related parameters

In our model, the insulator thickness  $d_1$  and its dielectric constant  $\epsilon_1$  of the touchscreen (rigid solid with the flat surface shown in Fig. 1) were determined for the capacitive touchscreen (Model: SCT-3250, 3M) used in our experiments (see Section 4). A field emission scanning electron microscopy (FESEM, Zeiss Ultra Plus) analysis was performed on the touchscreen to measure the thickness of the insulating layer. Fig. 8 presents a cross-sectional FESEM image of the touchscreen. The image on the left is acquired by the secondary electron detector and displays the topography. The image on the right is simultaneously collected with the in-lens detector and emphasizes the material contrast. The conductive layer appears with bright contrast whereas the top insulator layer appears in black. The image also shows that the top insulator has a different composition than the substrate glass. We identified 3 main layers through the measurement: electric insulator layer ( $\text{SiO}_2$ ) with a thickness of  $d_1 \approx 1$   $\mu\text{m}$ , electric conducting layer (ITO) with a thickness of  $\approx 250$  nm, and glass substrate. The dielectric constant of the insulator layer  $\epsilon_1 \approx 3.9 - 10$  is used below.<sup>44–46</sup> The effective thickness of the insulating layer  $h_0 = d_1/\epsilon_1 + d_2/\epsilon_2$  is not exactly known since the thickness  $d_2$  and the dielectric constant  $\epsilon_{SC}$  of the SC are highly dependent on the subject.<sup>47</sup>

### 3.3 Sliding friction experiments on touchscreen with human finger

The effect of the voltage applied to the conductive layer of the touchscreen on the friction force  $F_f$  was investigated as a function of the normal force applied to the touchscreen by the sliding index finger, and the results were compared with those obtained from theory.

The major components of our set-up include a high-torque step motor moving a slider on a power screw and a force sensor attached to the base of the touchscreen (Model: SCT-3250, 3M)

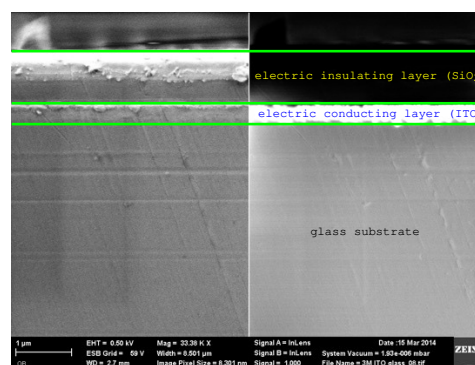


**Fig. 8** A cross-sectional image of the capacitive touchscreen (Model: SCT-3250, 3M) obtained by field emission scanning electron microscopy (FESEM, Zeiss Ultra Plus). The image on the left shows the layers of the touchscreen. The image on the right is collected simultaneously by its in-lens detector to obtain a better contrast for differentiating the layers. There are three main layers: electric insulator layer ( $\text{SiO}_2$ ) with a thickness of  $\approx 1$   $\mu\text{m}$ , electric conducting layer (ITO) with a thickness of  $\approx 250$  nm, and glass substrate.

are shown in Fig. 9. The step motor (MDrive23Plus, Intelligent Motion Systems Inc.) was programmed to translate the slider forward and backward in horizontal direction at the desired sliding velocity. The experimenter's hand was placed on the slider such that the phalanges of index finger were aligned with a constant angle of approximately  $30^\circ$  with respect to the touchscreen, and the tip of the index finger was always in contact with the touchscreen during the sliding. A sinusoidal voltage signal with each of the following amplitudes 25 V, 50 V, 75 V, 100 V, 125 V, 150 V, 175 V, and 200 V at 125 Hz was applied to the touchscreen. As the experimenter's finger was moving on the touchscreen, the force response was measured using a force transducer (Nano 17, ATI Industrial Automation Inc.) placed under the touchscreen. The normal and tangential forces were acquired by a 16-bit analog data acquisition card (NI PCI-6034E, National Instruments Inc.) with a sampling rate of 10 kHz. Note that the electric stress oscillates between zero and a value twice as large as the average electric stress, although the voltage applied to the touchscreen

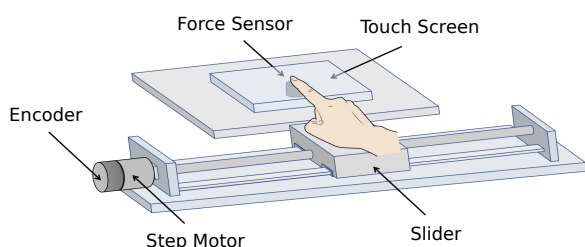


**Fig. 9** The experimental setup used to measure the force response of the index finger in the normal and tangential directions via a force transducer (Nano 17, ATI Industrial Automation Inc.) placed under the touchscreen (Model: SCT-3250, 3M) as a function of applied voltage  $V$ . The experimenter's hand was placed on the slider driven by a step motor (MDrive23Plus, Intelligent Motion Systems Inc.) such that the phalanges of index finger were aligned with an angle of approximately  $30^\circ$  with respect to the touchscreen, and the tip of the index finger was always in contact with the touchscreen during the forward and backward translation of the slider along the horizontal direction.

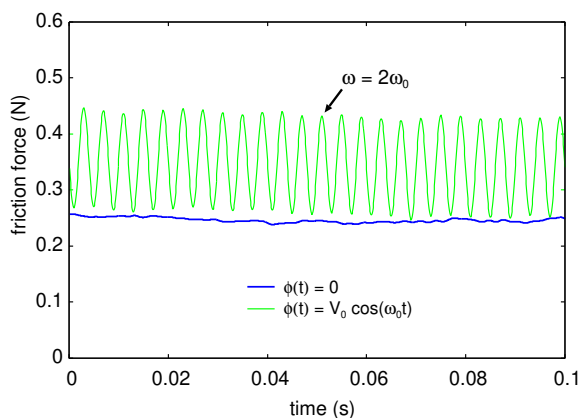


**Fig. 10** The friction force  $F_f$  as a function of time. Green-colored data: with an applied oscillating electric potential  $\phi(t) = V_0 \cos(\omega_0 t)$  ( $V_0 = 100$  V and  $f_0 = \omega_0/(2\pi) = 125$  Hz). Blue-colored data: without an applied electric potential. The normal force is  $F_N = 1$  N in both cases. Note that there are 25 oscillations in the green-colored data, i.e., the frequency of oscillations in the electric stress is  $25/0.1 = 250$  Hz, i.e., twice the frequency of the applied electric potential.

takes negative and positive values, and oscillates around zero. If we assume that the friction force  $F_f$  is proportional to the sum of the applied stress  $p_0$  and the adhesive stress (3), then we expect the friction force to oscillate with the frequency  $2\omega_0$ , where  $\omega_0$  is the frequency of the voltage signal applied to the touchscreen.

To illustrate that this is indeed the case, in Fig. 10 we show the measured friction force  $F_f$  as a function of time. The green-colored data is with the applied oscillating electric potential  $\phi(t) = V_0 \cos(\omega_0 t)$  ( $V_0 = 100$  V and  $\omega_0 = 2\pi f_0$  with  $f_0 = 125$  Hz) while the blue-colored data is the friction force without an applied electric potential. The blue-colored data is slightly below the green one because the applied normal force was slightly lower in the case of no applied voltage.

The finger of the experimenter moved forward and backward on the touchscreen for a total displacement of 80 mm in one cycle. The sliding velocity was selected as 50 mm/s based on the preliminary experiments such that full slip behavior was observed between the fingertip and the touchscreen. For each applied voltage, the experimenter aimed to increase his normal force from 0.2 N to 2 N with an increment of 0.2 N after every other 4 cycles. In order to keep the normal force constant, the test person visually tracked his force response from a large screen oscilloscope and trained himself in advance of the experiments. However, it is important to emphasize that keeping the normal force at a constant value was not easy even for a trained experimenter and some deviations occurred. The electrovibration was turned on and off after every other cycle. Hence, the experimenter made a total number of 320 cycles (8 different applied voltages  $\times$  10 increments of normal force per applied voltage  $\times$  2 cycles per force increment  $\times$  2 experimental condition (i.e., electrovibration on versus off).

All the experiments were carried out at the room temperature ( $22^\circ\text{C}$ ). The fingerpad of the subject and the glass of the touchscreen were cleaned with ethanol before each measurement. An external fan, placed near the sliding mechanism, was used to hinder the accumulation of moisture on the fingerpad.

## 4 Theory: Numerical results

Let us now present some numerical results. We assume that the skin is in contact with a touchscreen. The touchscreen is assumed to consist of a conducting layer covered by a thin insulating layer (thickness  $d_1$ ) as in Fig. 1. In the theory section, we have defined the effective thickness of the insulating layers as  $h_0 = d_1/\epsilon_1 + d_2/\epsilon_2$ . Assuming  $d_1 = 1$   $\mu\text{m}$  and that the insulating layer is made of silicone dioxide so that  $\epsilon_1 \approx 3.9$ , we get  $d_1/\epsilon_1 \approx 0.26$   $\mu\text{m}$ . If we assume that the SC has the thickness  $d_2 \approx 200$   $\mu\text{m}$ , and the dielectric constant  $\epsilon_2 \approx 3000$  (see Fig. 7), we get  $d_2/\epsilon_2 \approx 0.07$   $\mu\text{m}$ .<sup>47,48</sup> For the frequency  $f = 0$  (static)  $\epsilon_2 \approx 10^4$  giving  $d_2/\epsilon_2 \approx 0.02$   $\mu\text{m}$ . Thus, it appears that the insulating film on the substrate will give the largest contribution to  $h_0$ , and that it should be possible to reduce  $h_0$  to  $\approx 0.1$   $\mu\text{m}$  by reducing the thickness of the insulating film. In the following, unless otherwise stated, we will assume  $h_0 = 0.3$   $\mu\text{m}$  but we also show some results for  $h_0 = 0.1$   $\mu\text{m}$ , and  $h_0 = 1$   $\mu\text{m}$ . Hence, our reference system has the nominal values of  $h_0 = 0.3$   $\mu\text{m}$ ,  $d_2 = 200$   $\mu\text{m}$ ,  $E_{\text{bulk}} = 10$  kPa,  $E_{\text{SC}} = 100$  MPa, and the power spectrum given by the green curve



in Fig. 5 (which takes into account the plastic deformation). The applied squeezing pressure is  $p_0 = 10$  kPa, so finite size effects are unimportant (see Appendix A). In each of the following subsections, we investigate the influence of one parameter while fixing the others.

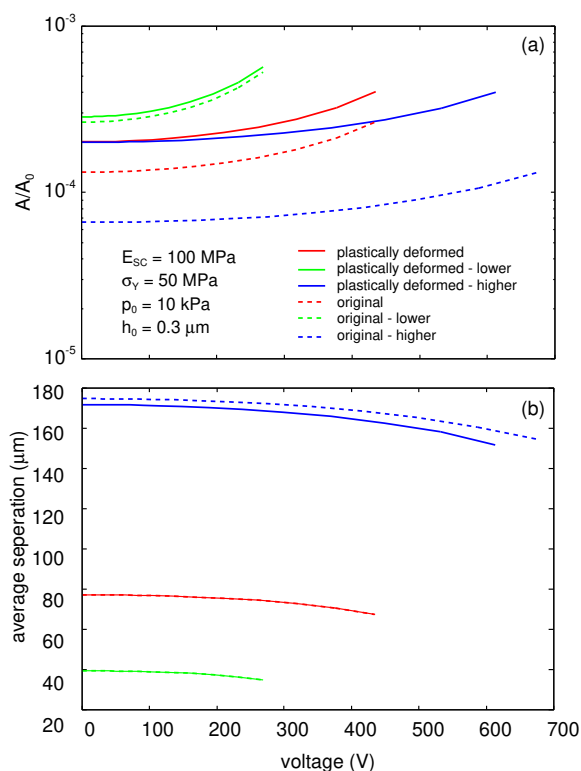


**Fig. 11** The normalized contact area  $A/A_0$  (a), and the average surface separation  $\bar{u}$  (b), as a function of the applied voltage  $V$ . We have used the surface roughness power spectrum shown in Fig. 5 (rms roughness =  $22$   $\mu\text{m}$ ), and those with 4 times higher and 4 times lower surface roughness (rms roughness =  $44$   $\mu\text{m}$  and  $11$   $\mu\text{m}$ , respectively). We assumed the Young's modulus of the SC as  $E_{SC} = 100$  MPa without plasticity (dashed curves) and with plasticity considering a penetration hardness of  $\sigma_Y = 50$  MPa (solid curves). The thickness of the effective insulating layer is  $h_0 = d_1/\epsilon_1 + d_2/\epsilon_2 = 0.3$   $\mu\text{m}$ . The Young's modulus of the bulk material is  $E_{\text{bulk}} = 10$  kPa. The applied pressure is  $p_0 = 10$  kPa. Note that the curves of average separation for plastically deformed (solid red) and original (dashed red), and also plastically deformed - lower (solid green) and original - lower (dashed green) overlap (bottom figure).

#### 4.1 Power spectrum $C(q)$

Fig. 11 shows the normalized contact area  $A/A_0$ , and the average surface separation  $\bar{u}$  as a function of the applied voltage  $V$  for the surface roughness power spectrum shown in Fig. 5 (green curve), and those with 4 times higher and 4 times lower power spectrum (solid and dashed red curves). The thickness of the effective insulating layer is  $h_0 = d_1/\epsilon_1 + d_2/\epsilon_2 = 0.3$   $\mu\text{m}$ . The results show an increase in the normalized contact area  $A/A_0$ , when the power spectrum of the plastically deformed surface (solid red) is used, compared to that without plastic deformation (dashed red). On the other hand, the normalized contact area  $A/A_0$  is decreased when the surface rms-roughness is increased. The average separation between the surfaces has a negative correlation

with the normalized contact area  $A/A_0$ . As expected, the average separation between the surfaces is reduced as the rms roughness amplitude is lowered.

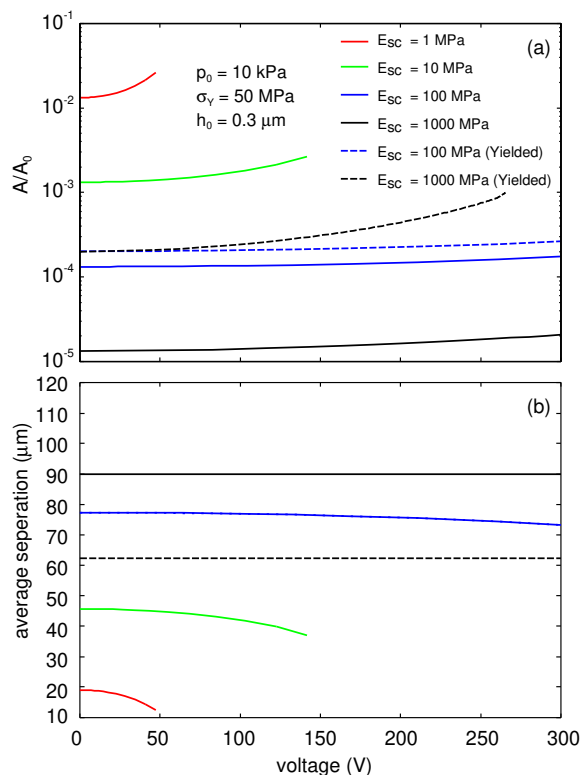


**Fig. 12** The normalized contact area  $A/A_0$  (a), and the average surface separation  $\bar{u}$  (b), as a function of the applied voltage  $V$ . The Young's modulus of the SC is taken as  $E_{SC} = 1$  MPa (red),  $E_{SC} = 10$  MPa (green),  $E_{SC} = 100$  MPa (blue),  $E_{SC} = 1000$  MPa (black),  $E_{SC} = 100$  MPa with plasticity, assuming a penetration hardness of  $\sigma_Y = 50$  MPa (dashed blue) and  $E_{SC} = 1000$  MPa with plasticity, assuming a penetration hardness of  $\sigma_Y = 50$  MPa (dashed black). The thickness of the effective insulating layer is  $h_0 = d_1/\epsilon_1 + d_2/\epsilon_2 = 0.3$   $\mu\text{m}$ . The Young's modulus of the bulk material is  $E_{\text{bulk}} = 10$  kPa. The applied pressure is  $p_0 = 10$  kPa. Note that the curves for  $E_{SC} = 100$  MPa (blue) and  $E_{SC} = 100$  MPa (yielded, dashed blue) overlap on top of each other at the bottom figure.

#### 4.2 Young's modulus $E_{SC}$ of the SC

Fig. 12 shows the normalized contact area  $A/A_0$  (a), and the average surface separation  $\bar{u}$  (b), as a function of the applied voltage  $V$ . The thickness of the effective insulating layer is  $h_0 = d_1/\epsilon_1 + d_2/\epsilon_2 = 0.3$   $\mu\text{m}$ , the Young's modulus of the bulk material is  $E_{\text{bulk}} = 10$  kPa, and the applied pressure is  $p_0 = 10$  kPa. The results demonstrate that when the Young's modulus of the SC increases, the normalized contact area  $A/A_0$  decreases, while the average surface separation  $\bar{u}$  increases. Enabling plasticity for  $E_{SC} = 1$  GPa results in an increase in the normalized contact area and a decrease in the average surface separation.

#### 4.3 Thickness $d_2$ of the SC

In order to evaluate the effect of the SC thickness on the normalized contact area  $A/A_0$ , and the average surface separation  $\bar{u}$  as a function of the applied voltage  $V$ , simulations are performed us-

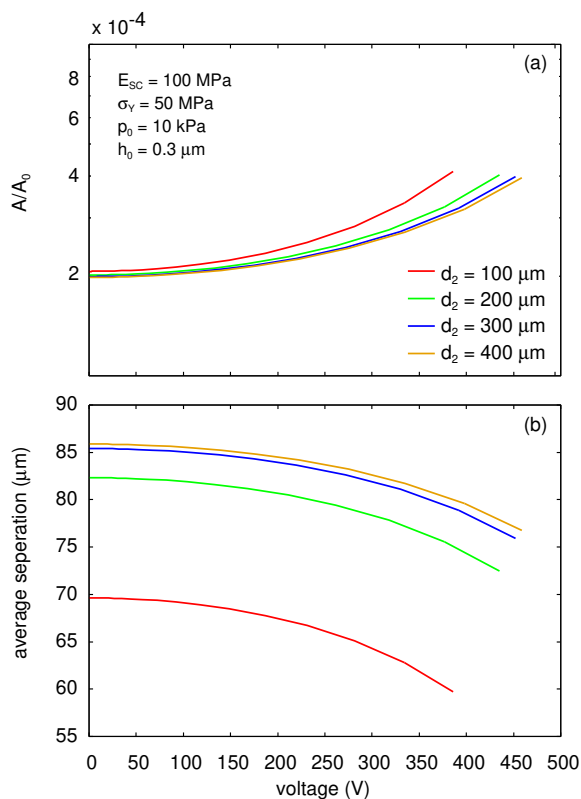


**Fig. 13** The normalized contact area  $A/A_0$  (a), and the average surface separation  $\bar{u}$  (b), as a function of the applied voltage  $V$ . The thickness of the SC is  $d_2 = 100 \mu\text{m}$  (red),  $d_2 = 200 \mu\text{m}$  (green),  $d_2 = 300 \mu\text{m}$  (blue), and  $d_2 = 400 \mu\text{m}$  (yellow). The Young's modulus of SC is  $E_{\text{SC}} = 100 \text{ MPa}$ , penetration hardness is  $\sigma_Y = 50 \text{ MPa}$ , the power spectrum is the green curve in Fig. 5, and the Young's modulus of the bulk material is  $E_{\text{bulk}} = 10 \text{ kPa}$ .

ing the thickness values reported in the literature.<sup>48</sup> The Young's modulus of the SC is taken as  $E_{\text{SC}} = 100 \text{ MPa}$  with the power spectrum shown by the green curve in Fig. 5, the applied pressure is  $p_0 = 10 \text{ kPa}$ , and the thickness of the effective insulating layer is  $h_0 = d_1/\varepsilon_1 + d_2/\varepsilon_2 = 0.3 \mu\text{m}$ . Fig. 13 shows that when the thickness of the SC decreases, the normalized contact area  $A/A_0$  increases while the average surface separation decreases.

#### 4.4 Effective thickness $h_0$ of insulating layer

Fig. 14 shows the influence of the thickness of the effective insulating layer  $h_0$  on the normalized contact area  $A/A_0$ , and the average surface separation  $\bar{u}$  as a function of the applied voltage  $V$ . The thickness of the effective insulating layer is varied based on the possible variations in the parameters of  $h_0 = d_1/\varepsilon_1 + d_2/\varepsilon_2$ . The Young's modulus of the SC is taken  $E_{\text{SC}} = 100 \text{ MPa}$  with the power spectrum shown by the green curve in Fig. 5, and the applied pressure is  $p_0 = 10 \text{ kPa}$ . The results show that the thickness of the effective insulating layer has a significant impact on the normalized contact area and the average surface separation for the values varying between  $h_0 = 0.1 - 0.4 \mu\text{m}$ . As  $h_0$  is decreased, the normalized contact area is enlarged, while the average surface separation is reduced.

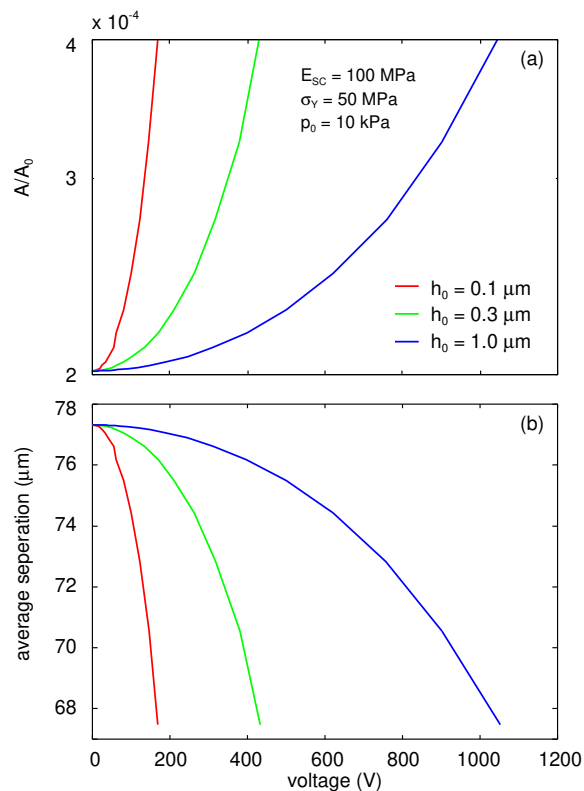


**Fig. 14** The normalized contact area  $A/A_0$  (a), and the average surface separation  $\bar{u}$  (b), as a function of the applied voltage  $V$ . The thickness of the effective insulating layer is taken as  $h_0 = d_1/\varepsilon_1 + d_2/\varepsilon_2 = 0.1 \mu\text{m}$  (red),  $0.3 \mu\text{m}$  (green) and  $1 \mu\text{m}$  (blue). The Young's modulus of SC is  $E_{\text{SC}} = 100 \text{ MPa}$  with plasticity (penetration hardness  $\sigma_Y = 50 \text{ MPa}$ ), assuming the power spectrum shown by the green curve in Fig. 5. The Young's modulus of the bulk material is  $E_{\text{bulk}} = 10 \text{ kPa}$ , the applied pressure is  $p_0 = 10 \text{ kPa}$ .

#### 4.5 Applied nominal contact pressure $p_0$

The influence of the applied contact pressure  $p_0$  on the the normalized contact area  $A/A_0$ , and the average surface separation  $\bar{u}$  are shown in Fig. 15. The contact pressure is selected in the range of  $p_0 = 1 - 100 \text{ kPa}$  based on the typical pressures applied by the finger to touchscreen. As expected, the results show that the normalized contact area increases with the applied contact pressure while the average surface separation decreases.

#### 4.6 Probability distribution of electro-adhesive stress

The contact between randomly rough surfaces result in physical quantities which fluctuate strongly depending on the location at the interface. In addition, some properties may differ for each realization of the system. In this case it is useful to consider the probability distribution of a property. The probability distribution for the interfacial separation, of the electric field strength in the gap, and of the interfacial stress acting on the solid walls, was presented in Ref.<sup>49</sup>. Here we consider the probability distribution of the attractive electric stress.

Let  $P_u(u)$  and  $P_\sigma(\sigma)$  be the probability distributions for the separation  $u$  and the attractive electric stress  $\sigma$  acting on the outer surface of the skin from the touchscreen. The probability distri-

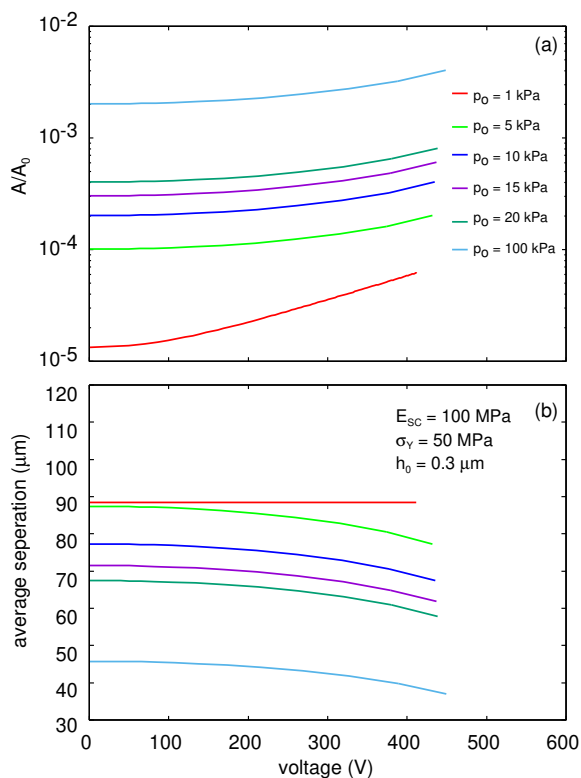


**Fig. 15** The normalized contact area  $A/A_0$  (a), and the average surface separation  $\bar{u}$  (b), as a function of the applied voltage  $V$ . The applied squeezing pressure  $p_0$  is varied in the range of  $p_0 = 1 - 100$  kPa. The thickness of the effective insulating layer is  $h_0 = d_1/\epsilon_1 + d_2/\epsilon_2 = 0.3$   $\mu\text{m}$ . The SC Young's modulus is  $E_{SC} = 100$  MPa with plasticity (penetration hardness  $\sigma_Y = 50$  MPa), assuming the power spectrum shown by the green curve in Fig. 5. The Young's modulus of the bulk material is  $E_{\text{bulk}} = 10$  kPa.

butions are assumed to be normalized so that, e.g.,

$$\int_0^\infty du P_u(u) = \int_0^\infty d\sigma P_\sigma(\sigma) = 1$$

Let us derive the distribution of attractive stress due to the electric field in the air gap. The electric stress

$$\sigma = \frac{1}{4} \frac{\epsilon_0 V_0^2}{(u + h_0)^2}. \quad (26)$$

Thus we get

$$d\sigma = -\frac{1}{2} \frac{\epsilon_0 V_0^2}{(u + h_0)^3} du.$$

From

$$\int_0^\infty du P_u(u) = \int_0^\infty d\sigma P_\sigma(\sigma) = \int_0^\infty du P_\sigma \frac{1}{2} \frac{\epsilon_0 V_0^2}{(u + h_0)^3}$$

we get

$$P_\sigma = \frac{2(u + h_0)^3}{\epsilon_0 V_0^2} P_u \quad (27)$$

Using (26) and (27) it is easy to plot  $P_\sigma$  as a function of  $\sigma$  given  $P_u$  as a function of  $u$ .

Fig. 16(a) shows the probability distribution of the adhesive electric stress acting on the outer skin surface in the nominal skin-

glass contact area. In most of the skin area the adhesive stress is very small, of order 1 – 100 Pa, but this surface area gives a negligible contribution to the total attractive electrostatic force. This can be shown as follows:

To understand which region in space gives the biggest contribution to the electric adhesion force we consider the average adhesive stress

$$\langle \sigma \rangle = \int_0^\infty d\sigma \sigma P_\sigma(\sigma)$$

Let us introduce a new integration variable  $x = \log_{10}(\sigma)$  so that  $d\sigma = \ln(10)\sigma dx$  and

$$\langle \sigma \rangle = \int_{-\infty}^\infty dx S(x),$$

where

$$S = \ln(10)\sigma^2 P_\sigma(\sigma).$$

Thus  $S(x)dx$  is the contribution to the average stress from the region where the logarithm of the stress is between  $x = \log_{10}\sigma$  and  $x + dx = \log_{10}\sigma + d\log_{10}\sigma$ . In Fig. 16(b) we show  $\log_{10}S$  as a function of  $x = \log_{10}\sigma$ . Clearly the most important contribution to the adhesive normal load comes from the region where the stress is close to the maximum stress  $\sigma_{\text{max}} = \epsilon_0 V_0^2 / (4h_0^2)$  indicated by the vertical dashed line. This region in  $\sigma$ -space corresponds to the area of real contact and the region close to the area of real contact, where the skin-touchscreen surface separation is very small; this region is denoted as the rim-area.

## 5 Comparison of the theory with the experiment

The friction force  $F_f$  and the normal force  $F_N$  (markers) measured as a function of the applied voltage  $V$  are presented in Fig. 17. The voltage between the conductive layer of the touchscreen varies from 0 V to 200 V with an increment of 25 V at 125 Hz. The results show that the friction force was increased with the normal force for the range of  $F_N = 0.2 - 2$  N. Also, the friction force increases when the applied voltage is increased. Note that the relative increase in the friction force with voltage is in good agreement with the theory suggesting that electrostatic force is proportional to the square of the applied voltage.

We also measured the apparent contact area of the fingertip of the experimenter at different normal loads from the high-contrast fingerprint images obtained by a coaxial light source and camera. The apparent contact area  $A_0$  depends weakly on the normal force  $A_0 \sim F_N^{0.1}$ . Since we argue that the real contact area is more important than the nominal contact area for the contact mechanics and friction, we will not discuss the results any further here.

In the relevant range of nominal contact pressures, the theory predicts that the relative contact area  $A/A_0$  is nearly proportional to the applied nominal contact pressure  $p_0$ . Assume that the frictional shear stress  $\tau_f$  acting on the area of real contact is independent of  $p_0$ , as expected from the theory when the local pressure in the asperity contact regions is small enough, or when the pressure in the contact regions is nearly constant. In this case, it follows that the friction force  $F_f = \tau_f A = \tau_f (A/A_0) A_0$  is nearly proportional to the normal force  $F_N = A_0 p_0$ , and we can obtain the relation

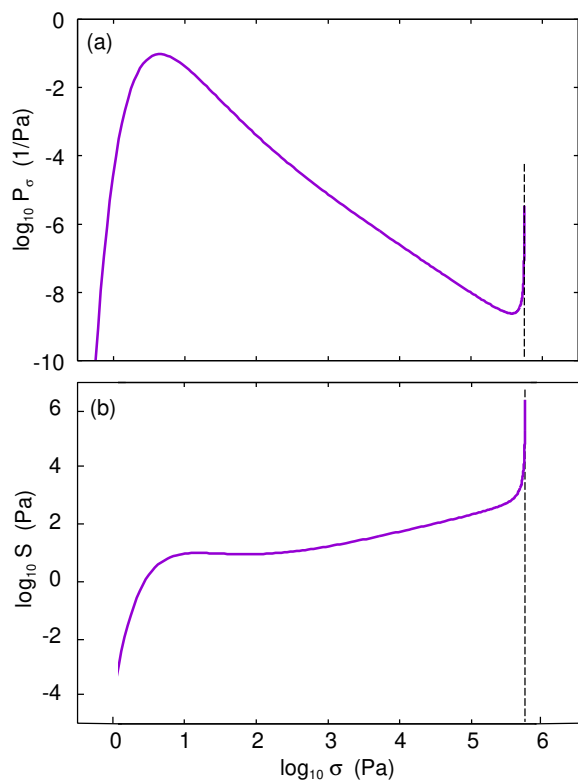


**Fig. 16** (a) The probability distribution  $P_\sigma(\sigma)$  of the electric attraction stress. The logarithm of  $P_\sigma(\sigma)$  is shown as a function of the logarithm of the electric stress. (b) The logarithm of the function  $S$  as a function of the logarithm of the electric stress (see text for details). The vertical dashed line indicate the maximum electric stress  $\sigma = \epsilon_0 V_0^2 / (4h_0^2)$ . For  $E_{SC} = 40$  MPa,  $h_0 = 0.2$   $\mu\text{m}$ , the applied voltage amplitude  $V_0 = 100$  V.

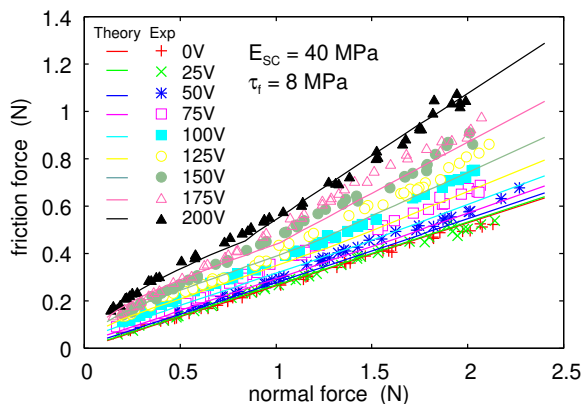


**Fig. 17** The friction force  $F_f$  obtained from the theory (solid curves) and the experiments (markers) as a function of the applied normal force  $F_N$ . The voltage applied to the conductive layer of the touchscreen is varied from 0 V to 200 V with an increment of 25 V at 125 Hz. The speed of the sliding finger during the experiments was 50 mm/s. In the model, we set  $E_{SC} = 40$  MPa,  $d = 200$   $\mu\text{m}$ ,  $E_{\text{bulk}} = 10$  kPa and  $h_0 = 0.2$   $\mu\text{m}$ . Shear stress is assumed to be  $\tau_f = 8$  MPa, which is consistent with  $\tau_f = 5$  MPa for wet skin and  $\tau_f = 13$  MPa for dry skin.<sup>30,31</sup>

between  $F_f$  and  $F_N$  directly from the relation between  $A/A_0$  and  $p_0$ .

In Fig. 17 we compare the friction force  $F_f$  measured as a function of the normal force with the one predicted by the theory

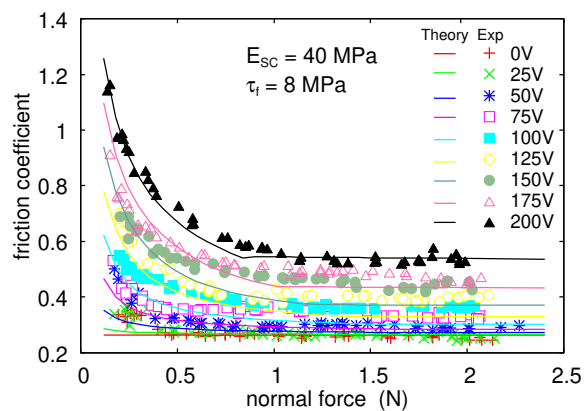


**Fig. 18** The friction coefficient  $\mu$  obtained from the theory (solid curves) and the experiments (markers) as a function of the applied normal force  $F_N$ . The voltage applied to the conductive layer of the touchscreen is 0 V (red) and 200 V (black). Based on the experimental and theoretical data presented in Fig. 17.

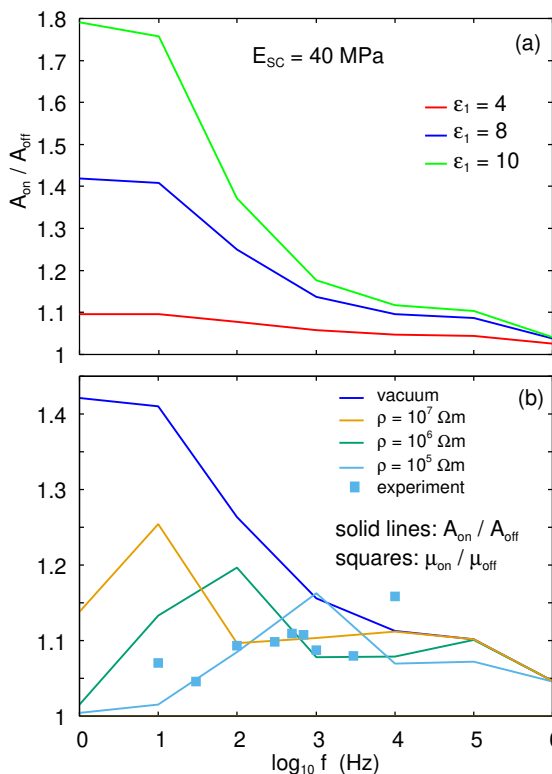


**Fig. 19** The calculated dependency of the contact area on the frequency  $f = \omega / (2\pi)$  of the oscillating electric potential  $\phi = V_0 \cos(\omega t)$ . The  $A_{\text{on}}/A_{\text{off}}$  is the ratio between the real contact area with electroadhesion to that without electroadhesion, obtained using (10) with the dielectric function  $\epsilon_2(\omega)$  of the SC given by (13) with  $\epsilon_{SC}(\omega)$  and  $\rho_{SC}(\omega)$  given in Fig. 7. We have used the normal force  $F_N = 0.5$  N and  $V_0 = 100$  V,  $d_1 = 1$   $\mu\text{m}$ ,  $d_2 = 200$   $\mu\text{m}$ . In (a) we show results for  $\epsilon_1 = 4, 8$  and  $10$  assuming a vacuum (or air) gap, while in (b)  $\epsilon_1 = 8$  and the gap between the solids has a nonzero electric conductivity so that the charge on the skin surface can drift out on the touchscreen.

(solid curves). The frictional shear stress  $\tau_f$  was adjusted to obtain the best possible fit with respect to the measured data, and the value used for that,  $\tau_f = 8$  MPa, is consistent with  $\tau_f = 5$  MPa



for wet skin and  $\tau_f = 13$  MPa for dry skin.<sup>30,31</sup>

Note that when the electroadhesion is on, the measured friction force extrapolates to a finite value as the applied normal force extrapolates to zero. In the present case, this is due to finite-size effect: A finite system has asperities of finite height, and the average surface separation is finite even as the normal force approaches to zero. Hence, when the electroadhesion is on, there will always be an attractive force acting between the solids and a finite area of real contact, which results in non-zero friction force during sliding.

In Fig. 18 we show the friction coefficient obtained from the theory (solid curves) and the experiments (markers) as a function of the applied normal force  $F_N$ . The voltage applied to the conductive layer of the touchscreen is 0 V (red) and 200 V (black). The figure is based on the experimental and theoretical data presented in Fig. 17. Note that the friction coefficient increases when the applied normal force decreases.<sup>50</sup> This is a typical behavior when adhesion is important. Note that a small increase in the friction coefficient is also obtained when the applied voltage is turned off. This has been observed also in the earlier studies,<sup>38</sup> and must be due to some additional adhesion process, e.g., due to the van der Waals interaction, or due to capillary bridges formed by moisture or oil on the finger.<sup>21</sup> Since electroadhesion is the only attractive interaction included in the theory, the increase in friction coefficient as the applied normal force approaches to zero for  $V = 0$  cannot be described by the proposed theory yet.

Fig. 19 shows the calculated dependency of the contact area on the frequency  $f = \omega/(2\pi)$  of the oscillating electric potential  $\phi = V_0 \cos(\omega t)$ . The ratio  $A_{\text{on}}/A_{\text{off}}$  between the real contact area with electroadhesion to that without electroadhesion was obtained using (10) with the dielectric function  $\epsilon_2(\omega)$  of the SC given by (13) with  $\epsilon_{\text{SC}}(\omega)$  and  $\rho_{\text{SC}}(\omega)$  given in Fig. 7. We have used the normal force  $F_N = 0.5$  N and  $V_0 = 100$  V,  $d_1 = 1$   $\mu\text{m}$ ,  $d_2 = 200$   $\mu\text{m}$ . Fig. 19(a) shows  $A_{\text{on}}/A_{\text{off}}$  for three different touchscreen glass dielectric constants,  $\epsilon_1 = 4, 8$  and  $10$ .

At low frequencies the charge on the skin surface can drift out on the touchscreen. This effect depends on the surface and bulk electric conductivity of the touchscreen, and on liquids (e.g. oil and sweat) which may occur in some fraction of the non-contact area. To take this into account we also show calculated results in Fig. 19(b) where we assume the airgap is filled with a material with the resistivity  $\rho$  equal to  $10^5, 10^6$  and  $10^7$   $\Omega$  m.

If we assume that the friction force is proportional to the area of real contact, then the ratio  $A_{\text{on}}/A_{\text{off}}$  equal the ratio  $\mu_{\text{on}}/\mu_{\text{off}}$  between the friction coefficient with electroadhesion to that without electroadhesion. The square symbols in Fig. 19(b) are experimental data for the ratio  $\mu_{\text{on}}/\mu_{\text{off}}$ . Similar results was obtained by Meyer et al.<sup>1</sup> (see also Ref.<sup>51</sup> for measurements using current controlled induction).

Note that as the frequency  $\omega$  decreases, the mobile charges on the skin will move from the inner interface between the SC and the tissue below, to the outer SC-air (or SC-glass) interface. In Sec. 2.2, we showed that this occurs on the time scale of  $\tau \approx \epsilon_0 \rho_{\text{SC}} \epsilon_{\text{SC}} \approx 3 \times 10^{-4}$  s (where we used the typical values  $\epsilon_{\text{SC}} \approx 2 \times 10^3$  and  $\rho_{\text{SC}} \approx 2 \times 10^4$   $\Omega\text{m}$ ) or for the frequency of  $f \approx 1/\tau \approx 10^3$  Hz. When the charges move to the outer SC-air

interface the average separation between the charges located on the glass surface and the outer SC decreases, and in order for the electric potential difference to stay constant, the electric field strength and hence the electroadhesion must increase as the frequency decreases as shown in Fig. 19(a).

Some experiments indicate that as the frequency decreases the electroadhesion force decreases (see Fig. 19(b)). This effect was observed by Meyer et al.<sup>1</sup> and may result from a drift of charges from the outer SC to the surface of the touchscreen [this effect depends on the surface and bulk electric conductivity of the glass], which results in a reduction in the electroadhesion as in Fig. 19(b) (see also Fig. 20). The transfer of charges from the outer SC to the surface of touchscreen could be strongly affected by ion drift motion in fluid (sweat) and capillary bridges formed between the finger skin and the touchscreen.

In the theoretical calculations, we took the SC Young's modulus  $E_{\text{SC}} = 40$  MPa, which corresponds to semi-wet skin. If a modulus value less than 40 MPa was taken, the electroadhesion would be larger. This could explain the fluctuations in the measured  $\mu_{\text{on}}/\mu_{\text{off}}$  typically observed in experimental measurements.

## 6 Discussion

While the technology for generating tactile feedback on a touchscreen via electrovibration (i.e. electroadhesion under an oscillating electric field) is already in place and straightforward to implement, our knowledge on contact mechanics for electroadhesion is highly limited. In particular, we still do not know the exact mechanism leading to an increase in tangential frictional forces under electroadhesion. In order to better understand the contact mechanism between the finger pad and touchscreen under electrovibration, we investigated the sliding friction as a function of normal force and the voltage applied to a touchscreen by means of a mean-field theory (Sec. 4) and experiments performed by a custom-made tribometer (Sec. 5). Some aspects of these three topics are further discussed in the following subsections.

### 6.1 Skin Model

The human skin is a multilayer composite material characterized by non-homogeneous, anisotropic, and non-linear properties, and with surface roughness extending over many decades in length scale. In our model, it is assumed that the layer below the SC has uniform mechanical properties and is treated as a linear elastoplastic material. In fact, even a linear viscoelastic model cannot fully describe the response of the skin to external forces. For a linear viscoelastic solid, if an indenter is pressed into its surface for some time period  $t_0$ , then the deformations will disappear after a time period of similar order once the indenter is removed. It is easy to test that this is not the case for the human skin: Fig. 21 shows an optical picture taken  $\approx 10$  minutes after a cylinder shaped indenter with a diameter of  $\approx 3$  mm and a wall thickness of  $\approx 0.5$  mm was pressed into the human wrist skin for  $\approx 3$  s with the nominal contact pressure of  $p_0 \approx 1$  MPa. The existence of deformations observed even after 10 minutes may be due to fluid motion in poroelastic matrix, which cannot be described accurately using a linear viscoelastic model.<sup>52,53</sup>

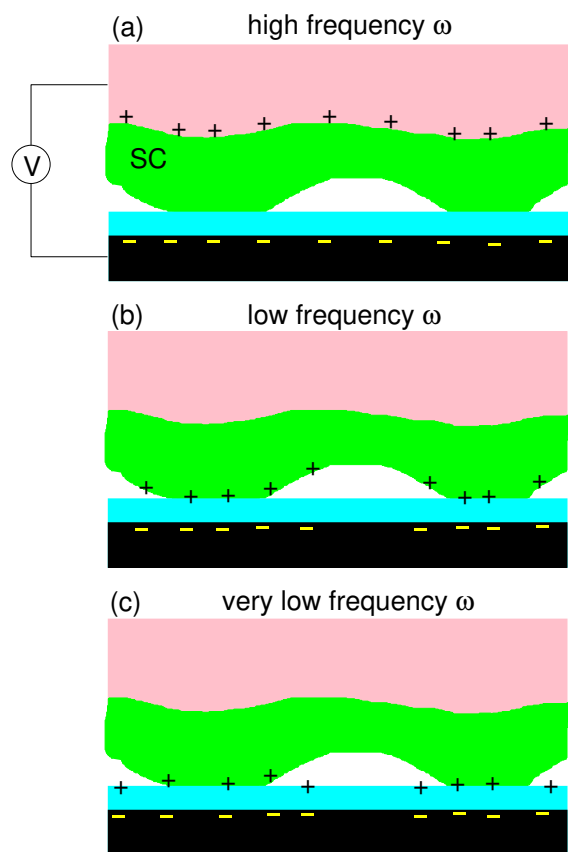


**Fig. 20** Distribution of charges at the contact between the skin (green and pink) and a touchscreen (black and blue) when an oscillating electric potential  $\phi = V_0 \cos(\omega t)$  acts between the skin and the touchscreen. The SC of the skin (green) has a finite electric conductivity. (a) When the frequency  $\omega$  is very high there is not enough time for charges to drift through the SC during the time period of an oscillation  $T = 2\pi/\omega$ . (b) As  $\omega$  decreases, charges can drift to the outer surface of the SC. If the electric resistance of the surface of touchscreen is infinite, no charges can flow to it. (c) However, the surface of touchscreen has a finite surface conductivity, and if the frequency  $\omega$  is small enough, the charges will drift to the surface of touchscreen, which will reduce the electroadhesive force between the finger and the touchscreen to nearly zero.

10 minutes after 3 sec long indentation by hollow cylindrical indenter



**Fig. 21** Optical picture taken 500 sec after a cylindrical shaped indenter with a diameter of  $\approx 3$  mm and wall thickness of  $\approx 0.5$  mm was pressed into the human wrist skin for  $\approx 3$  sec with the nominal contact pressure of  $p_0 \approx 1$  MPa

It is well-known that the friction coefficient of the human skin depends on many factors: 1) the material and physical properties of the skin such as Young's modulus, thickness of the layers, roughness and skin moisture level; 2) physiological conditions of the skin (e.g. age, gender, and ethnicity); 3) environmental conditions (e.g., temperature, humidity); 4) mechanical contact parameters (e.g., anatomical contact region, loading type, direction, speed and magnitude); and 5) contact interface properties (e.g., topologically applied substances and lubrication).<sup>48,54</sup> In this paper, we demonstrated that for a touchscreen providing electrostatic haptic feedback, the thickness and dielectric constant of the insulating layer of touchscreen, and the potential difference between the conducting layers also affect the sliding friction. Our numerical results reported in Sec. 4 demonstrate the effects of roughness, Young's modulus ( $E_{SC}$ ), thickness of the SC ( $d_2$ ), effective thickness of the insulating layers ( $h_0$ ), and applied nominal contact pressure ( $p_0$ ). Now, let us discuss and justify the parameters we used in these simulations.

### 6.1.1 Young's modulus $E_{SC}$ of the SC

Naturally, the skin has three functional layers: epidermis (top layer), dermis (middle layer) and subcutis (bottom layer). The material properties of each layer also depend on many factors (e.g., the anatomy of the skin of individual person, skin hydration, and measurement method). Several studies reported the elastic modulus of the SC (outermost electrically insulating layer of epidermis), dermis and subcutis in the ranges of 10 kPa – 1 GPa, 0.5 kPa – 45 MPa, and 0.12 kPa – 30 kPa, respectively.<sup>39–41</sup> The mechanical properties are strongly dependent on the environmental conditions: a decrease in the elastic modulus was observed with an increase in either relative humidity or temperature. Papir *et al.*<sup>47</sup> observed that the elasticity of the SC declines from 8.87 GPa at 26% RH to 2.44 GPa at 68% RH, and an order of magnitude decrease (12 MPa) was observed at 100% RH.

In our model, we assumed that the skin has only two layers: the top layer (SC), and the bulk layer: we varied the Young's modulus of SC in the range of  $E_{SC} = 1$  MPa – 1 GPa, and thickness of SC in the range of  $d_2 = 100$  – 400  $\mu\text{m}$  while keeping the elastic modulus of the bulk constant as  $E_{\text{bulk}} = 10$  kPa.

### 6.1.2 Power spectrum $C(q)$

Derler *et al.*<sup>54</sup> examined the friction coefficient of dry skin (index finger and edge of hand) against smooth (rms roughness  $\xi = 0.004$   $\mu\text{m}$ ) and rough ( $\xi = 2$   $\mu\text{m}$ ) glass, and showed that smoother surfaces have higher friction values than that of rough surfaces. Hendriks and Franklin<sup>55</sup> have further shown that the surface roughness of the indenting probe has a dominant affect on the friction coefficient: the smoother the probe surface, the higher the friction coefficient. This result can be explained by the increase in the contact area that would be observed at smoother roughness. On the other hand, for very rough surfaces, Tomlinson *et al.*<sup>56</sup> observed an increasing trend of friction coefficient for human finger with increasing material roughness ( $\xi = 1$  – 25  $\mu\text{m}$ ) and then a plateau ( $\xi = 25$  – 90  $\mu\text{m}$ ) for aluminum, brass, and steel. These results show two friction regimes for dry skin with increasing roughness: 1) the friction coefficient initially decreases

due to high real contact area at lower counter surface roughness and then 2) increases until it reaches to a steady state regime due to hysteresis, ploughing, and interlocking.<sup>38</sup> In our model (see Fig. 1), we assume a flat rigid solid surface for the counter surface and hence our findings in Fig. 11 are in an agreement with the first friction regime.

Persson *et al.*<sup>30</sup> measured the surface topography of dry human wrist skin using an optical method with a lateral resolution of 1  $\mu\text{m}$ . Later, Kovalev *et al.*<sup>31</sup> performed AFM measurements at a higher resolution, and combined their measurements with the optical measurements reported in the previous study. Hence, they obtained a surface roughness power spectrum covering over all relevant length scales and reported the rms roughness of the dry human skin as 22  $\mu\text{m}$ . In our work, we adopted the surface roughness power spectrum of the dry human skin from these studies, and also used 4 times higher and lower power spectrum in magnitude to consider subject-based variations. Overall, the surface spectrum roughness used in the numerical simulations were in agreement with those reported in the literature.

### 6.1.3 Thickness $d_2$ of the SC

The thickness of the SC of seven human subjects was determined to vary between 210 – 640  $\mu\text{m}$  by measuring the distance between the skin surface and the border of the living epidermis using optical coherence tomography,<sup>48</sup> while the thickness of isolated SC was measured to vary between 10 – 40  $\mu\text{m}$  in some other studies.<sup>40,41</sup> In the current study, we assumed that the skin has two layers: the top layer (SC), and the bulk below; and we varied the thickness of SC in the range of  $d_2 = 100 - 400 \mu\text{m}$  in our model.

### 6.1.4 Effective thickness $h_0$ of insulating layer

The dielectric constant of the insulating layer of the skin is highly dependent on the subject,<sup>47</sup> therefore we assumed the effective insulator thickness is in the range of  $h_0 = 0.1 - 1 \mu\text{m}$  to take these variations in the skin related parameters ( $d_2$  and  $\epsilon_2$ ) into the account. Derler *et al.*<sup>38</sup> measured the surface roughness ( $R_a$ ) of index finger skin to vary in the range of 6.8 – 43  $\mu\text{m}$  using a mechanical profilometer (Mahr, Perthometer M1). To our knowledge, no study has been performed to investigate the effect of the thickness of SC on the sliding friction of skin. Fig 13 shows the dependency of the SC thickness ( $d_2$ ) on the relative contact area ( $A/A_0$ ). Practically, we know that some users of touchscreen experience difficulties in sensing electroadhesion while some do not. This might be due to the thickened SC regions formed as a result of pressure and repeated wear, which leads to a lower relative contact area, and hence lower frictional force under electroadhesion. Also, the findings given in Fig. 14 are very important and show that the normalized contact area, and hence the frictional force can be increased significantly by modifying the effective thickness of the insulating layer of touchscreen. Based on our assumptions in this study, it appears that the thickness of the insulating film on the substrate have the largest contribution to  $h_0$ , and it is possible to reduce  $h_0$  down to  $\approx 0.1 \mu\text{m}$  for achieving stronger tactile effect.

### 6.1.5 Applied nominal contact pressure $p_0$

The measured friction coefficient of the skin is strongly dependent on the applied normal load. In the literature,<sup>38,42</sup> it has been re-

ported that the contact area and hence the friction force increases as the normal load applied by the human finger is increased. This result matches with our findings shown in Fig. 15.

### 6.1.6 Frictional shear stress $\tau_f$

Estimating the frictional shear stress  $\tau_f$  acting in the contact regions between a human finger and a touchscreen is difficult since it depends on contamination films (e.g., oil and water on the finger) and their composition and spatial distribution, which are not known in detail and vary from one individual to the next. We note, however, that the value used for frictional shear stress in our theoretical calculations is very close to what has been measured in earlier experimental studies on human finger-glass interaction under sliding.<sup>30,31</sup>

Unfortunately, the theoretical calculation of frictional shear stress under the conditions of boundary lubrication is a highly challenging task. Even in the most idealized situation with perfect smooth surfaces, no contamination films, and the exact knowledge about the atomic positions, it is almost impossible to accurately calculate the frictional shear stress using even a first principle theory like the density functional theory (or the less first-principle approach of molecular dynamics).

## 6.2 Tactile perception of electrovibration

One interesting observation is that the electroadhesion between a finger and a touchscreen can be felt only indirectly as a change (increase) in the sliding friction force. That is, when a stationary finger is gently pressed on the touchscreen, the electrovibration cannot be perceived. The reason for this is as follows: When a voltage is applied to the conductive layer of a touchscreen, an attractive stress will act on the skin in non-contact areas. The increase in total attractive force due to electroadhesion will be compensated by an increase in the repulsive force and the magnitude of total normal force acting on the finger (and on the touchscreen) will be unaltered (and equal to the applied normal force).

Blood and lymphatic vessels as well as most nerves and sensory receptors (for pain, pressure, touch etc.) are located in the dermis. However, since most of the electrovibration induced deformations in the skin is localized to the SC, the mechanoreceptors do not experience any stress to stimulate the spiking and convey information through nerve fibers to the brain. As a result, the electrovibration cannot be perceived when the finger is stationary. For sliding contact, instead, an additional friction force develops due to a change in real contact area between the finger and the touchscreen, which results in a fluctuating shear deformation on the finger. Hence, the Pacinian corpuscles (FA II receptors) which are sensitive to vibrations at frequencies varying between 5 – 500 Hz (main frequency of the friction signal was 250 Hz in our system, see Fig. 10) will be deformed and emit neural signals.<sup>57</sup> The discussion reported by Vardar *et al.*<sup>19</sup> is in agreement with our arguments given above where they suggested that Pacinian corpuscle is the primary psychophysical channel in the detection of the electrovibration stimuli.

## 7 Limitations of the study and further research questions

In this study, we have assumed that the only attraction between the finger and the touchscreen is the electrostatic force originating from the applied potential. In reality, there will always be other attractive interactions between two contacting solids, e.g. the Van der Waals interaction will operate between all solids and capillary bridges can be very important for the human skin. These additional interactions can be included in the future study. For example, the role of capillary bridges on adhesion was previously studied,<sup>21</sup> and a more general theory of adhesion was developed.<sup>22,58</sup>

In the theory presented above, we have neglected electrical breakdown across the narrow gap between the contacting solids.<sup>59</sup> When a large electric potential is applied between narrowly separated surfaces, a very large electric field can prevail, in particular close to high and sharp asperities. If the local electric field becomes larger than some critical value, breakdown occurs. For gap separations of  $\approx 1 \mu\text{m}$  or less, which is typical in many applications, the breakdown voltage is typically a few hundred volts.

Furthermore, the reason for the discrepancies between the experiments and theory shown in Fig. 17 might be due to the variations in the angle of contact made by the finger with touchscreen during the measurements, and changes in the hydration level of the skin due to the sweat and sebum excretion to the contact interface, which are highly challenging to control during the measurements.<sup>60</sup>

## 8 Conclusions

We have studied the contact mechanics between the human finger and a touchscreen when an electric potential exists between them. We have presented a detailed theoretical study of how the area of real contact and the friction force depend on contact parameters such as the nominal contact pressure and the applied voltage. For example, we show that when the Young's modulus of the SC is reduced due to finger moisture or increase in relative humidity in the environment, the separation between the finger and the touchscreen decreases, and hence the real contact area increases, which results in higher frictional forces acting on the finger during sliding. Our study shows that it is possible to increase the friction force by using a thinner insulating film on the touchscreen. We have also presented experimental data for how the friction force depends on the applied normal load and on the potential difference between the finger and the touchscreen. The experimental results were compared with the predictions made by the proposed theory, and a good agreement was observed. Finally, the dependency of the electroadhesion friction on the frequency of the oscillating electric potential has been investigated by using the proposed model and the results were compared with the recent experimental data reported in the literature.

## Conflicts of interest

There are no conflicts to declare.

## Acknowledgements

This work was performed within a Reinhart-Koselleck project funded by the Deutsche Forschungsgemeinschaft (DFG). BNJP would like to thank DFG for the project support under the reference German Research Foundation DFG-Grant: MU 1225/36-1. MS acknowledges COST Action CA15216 for grant STSM-CA15216-40485. MA and MS acknowledge FZ-Jülich for the support and the kind hospitality received during their visit to the PGI-1, where most of this work was performed. OS acknowledges the doctoral fellowship support provided by TUBITAK under BIDEB-2211 program. CB acknowledges the financial support provided by TUBITAK under the contract number of 117E954. Finally, the authors are grateful to Dr. Ozgur Birer from Koc University for the FESEM micrographs.

## Appendix A. Plastic deformation and finite-size effects

When solids with large elastic modulus and large surface roughness are squeezed into contact, the local pressure in asperity contact regions becomes so high that the softer material yields plastically. When the nominal contact pressure is small, the solids make contact in only a few macroasperity contact regions. In this case, one needs to take into account what we refer to as finite-size effects when calculating the distribution of interfacial separation. In this section, we will show that both of these effects are important for the contact between the human dry skin and a hard counter surface.

The elastic modulus of the SC depends on the relative humidity or wetness of the skin. Thus, dry skin has a Young's modulus of order  $E \approx 1 \text{ GPa}$ , as typical for glassy polymers. When the humidity increases,  $E$  decreases, such that at 100% relative humidity (wet state)  $E \approx 10 \text{ MPa}$ . The drop in the modulus with increasing humidity is due to the swelling and break-up of weak bonds (e.g., hydrogen bonds) in the skin by the water molecules, which lower the energetic barriers for rearranging segments of the polymer chains. This effectively convert the SC from a stiff glassy material to a soft rubbery material.

The drop in the Young's modulus of skin with increasing humidity is similar to the influence of temperature on the viscoelastic modulus of rubber. At low temperature (corresponding to dry skin) rubber is in the glassy state with a Young's modulus of order  $E \approx 1 \text{ GPa}$ . At high temperatures (corresponding to wet skin), it is in the rubbery state where the Young's modulus is in the order of a few MPa.

### Plastic deformation

Consider the contact between the human skin and a hard counter surface. When the elastic modulus of the SC is below  $\sim 100 \text{ MPa}$ , the contact pressures are typically below  $50 \text{ MPa}$  and we will assume that no plastic deformations occur on the SC. However, for dry skin,  $E > 1 \text{ GPa}$ , the stress in the asperity contact regions will be so high as to result in plastic deformation of the SC.

If an indenter is pushed into a linear viscoelastic solid for a certain period of time  $t_0$ , and then removed, the deformation will disappear after a time period of order  $t_0$ . This is not observed



for the human SC where the deformations need a longer time to disappear. This is similar to plastic deformation, but in contrast to plastic deformation of crystalline solids (e.g. metals), the deformation of the SC will slowly disappear after the external force field is removed. A more accurate model for the SC is a non-linear viscoelastic model of the following type: we assume that the external force pushes molecular groups (here polymer segments) over energetic barriers which are so large that thermal fluctuations require very long time to “move” the molecular groups back to the original minimum free-energy state (here undeformed state). This effect is well known for rubber materials below the glass transition temperature where plastic deformations induced by external forces will not disappear when the force field is removed even after a very long waiting time. However, if the rubber is warmed up to room temperature, the relaxation occurs and deformations rapidly disappear.<sup>43</sup> This shows that no strong covalent bonds break in the rubber during the deformations, as this would result in permanent (irreversible) changes in the molecular arrangements. Instead, the external forces move molecular segments from one position to another, and the energetic barriers separating the different geometrical arrangements of the polymer segments are too high to be overcome by thermal fluctuations at low temperatures, resulting in an apparent permanent plastic deformation of the rubber.

For the contact between elastoplastic solids, the concept of magnification is very important. When the interface is observed at the magnification  $\zeta$ , only roughness with wavenumber  $q < \zeta q_0$  is observed, where the  $q_0$  is the smallest wavenumber. If the contact pressure in the asperity contact regions observed at the magnification  $\zeta$  is below the penetration hardness  $\sigma_Y$ , the solid deforms elastically. However, when we increase the magnification, we observe more surface roughness at shorter length scales and the contact area decreases. As a result, the contact pressure in the asperity contact regions increases as  $\zeta$  increases. Finally, the contact pressure may be so high as to plastically deform the solid at short length scales.

When the compressive force is removed, the deformations on long length scale, which were elastic, will disappear. However, the short length scale deformations in the asperity contact regions by plastic flow will remain and effectively smooth out the solid surfaces in the asperity contact regions at short length scale. If the solids are compressed to make contact for a second time with the same normal force  $F_N$  as in the first contact, the solids deform purely elastically and the contact area can be obtained using the surface roughness power spectrum  $C_{pl}(q)$  of the (plastically) deformed surface. It was shown that  $C_{pl}$  can be obtained approximately using (with  $\zeta = q/q_0$ )

$$C_{pl}(q) = \left[ 1 - \left( \frac{A_{pl}(\zeta)}{A_{pl}^o} \right)^6 \right] C(q) \quad (26)$$

where  $A_{pl}^o = F_0/\sigma_Y$  ( $F_0$  is the normal load) is the contact area, assuming that all contact regions have yielded plastically so the pressure in all contact regions is equal to the penetration hardness.<sup>61,62</sup> The basic picture behind this definition is that surface roughness at short length scales gets smoothed out by plastic de-

formation, resulting in an effective cut-off of the power spectrum for large wave vectors (corresponding to short distances). The blue curve in Fig. 5 was obtained by using (26).

We now show numerical results illustrating the role of plastic deformations for dry skin. Fig. 22 shows the normalized contact area  $A/A_0$  as a function of the magnification  $\zeta = q/q_0$  (log-log scale) for the case  $E_{SC} = 1$  GPa and assuming the penetration hardness  $\sigma_Y = 50$  MPa.<sup>25</sup> We have assumed the thickness of the SC to be  $d_2 = 200$   $\mu\text{m}$ , and that the skin below the SC has the Young’s modulus  $E_{bulk} = 10$  kPa. The red curve shows the asperity contact area which is elastically deformed, and the green curve represents the area which is plastically deformed. The blue curve is the elastic contact area during a second contact with the plastically smoothed surface having the power spectrum given by the blue curve in Fig. 5.

Fig. 22 shows that assuming elastic contact and using the power spectrum (26) result in virtually the same contact area (numerically), as a function of magnification, as predicted for the original surface using the elastoplastic contact mechanics theory, where  $A(\zeta) = A_{el}(\zeta) + A_{pl}(\zeta)$ .

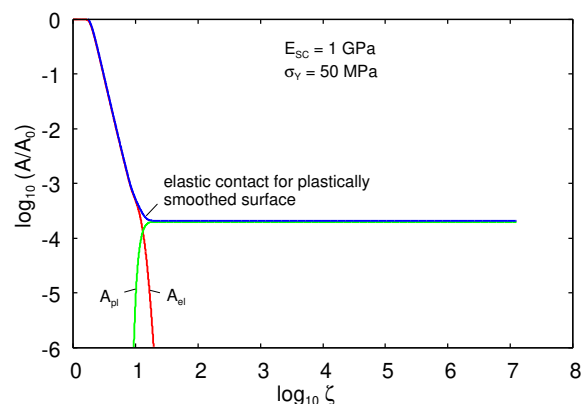


**Fig. 22** The normalized contact area  $A/A_0$  as a function of the magnification  $\zeta = q/q_0$  (log-log scale) for the case  $E_{SC} = 1$  GPa,  $\sigma_Y = 50$  MPa,  $d_2 = 200$   $\mu\text{m}$ , and  $E_{bulk} = 10$  kPa. The red curve is for the asperity contact area which is elastically deformed and the green curve is for the area which is plastically deformed. The blue curve is for the elastic contact area during a second contact with the plastically smoothed surface having the power spectrum given by the blue curve in Fig. 5.

### Finite size effect

Next, let us discuss what we refer to as finite size effects. Infinite solids with randomly rough surfaces have infinitely high asperities. In fact, such solids have a Gaussian height probability distribution, with a tail extending to infinite height. Analytical contact mechanics theories implicitly assume infinitely large surfaces and will therefore have infinitely many high asperities. However, real solids are finite and will always have the highest asperity; and when the separation between two solids is large enough, no contact will occur between the solids.

As long as the force squeezing two elastic solids together is large enough, many macroasperity contacts will occur, if, at least, the roughness power spectrum of one of the surfaces has a long wavelength roll-off region, as is the case for most surfaces of interest such as human skin. In that case, the contact mechanics for

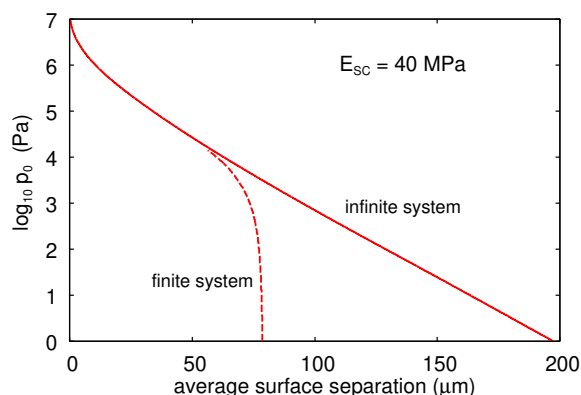


**Fig. 23** The logarithm of the nominal contact pressure  $p_0$  as a function of the average interfacial separation  $\bar{u}$  for the case  $E_{SC} = 40$  MPa. The solid curve is for the case of an infinite, randomly rough, surface (which has infinite high asperities) while the dashed curve is for a finite system with  $q_0 = 800 \text{ m}^{-1}$  corresponding to the length  $L = 2\pi/q_0 \approx 1$  cm. In the calculations, we have used the red-colored power spectrum shown in Fig. 5 with  $d_2 = 200 \text{ }\mu\text{m}$  and  $E_{\text{bulk}} = 10$  kPa. Note that finite-size effects are important when  $p_0 < p_c$  where  $p_c \approx 10^4$  Pa.

a finite and an infinite system, with randomly rough surfaces having the same statistical properties, will be nearly the same. However, for small applied normal force, this is not the case, and we refer to this as finite-size effect. Here, we note that the relation between the applied nominal contact pressure and the average surface separation is very different when the squeezing pressure is in the finite size regime, as compared to higher squeezing pressures. This topic has been already studied in depth,<sup>24,53</sup> and here we only show numerical results relevant to the human skin.

Fig. 23 shows the logarithm of the nominal contact pressure  $p_0$  as a function of the average interfacial separation  $\bar{u}$  for the case  $E_{SC} = 40$  MPa (semi-wet skin). The solid line is for the case of an infinite, randomly rough surface (which has infinitely many high asperities), while the dashed line is for a finite system with  $q_0 = 800 \text{ m}^{-1}$  corresponding to the length scale of  $L = 2\pi/q_0 \approx 1$  cm, which is a typical diameter for the apparent contact area between a fingerpad and a touchscreen. In the calculations, we have used the red-colored power spectrum shown in Fig. 5 and assumed  $d = 200 \text{ }\mu\text{m}$ ,  $E_{\text{bulk}} = 10$  kPa. Note that the finite-size effects are important when  $p_0 < p_c$  where  $p_c \approx 10^4$  Pa.

In this paper, we have included the finite size effects in the following way: since  $\bar{u}$  changes rather slowly with the contact pressure for  $p_0 < p_c$  (see the dashed line in Fig. 23) we use the same probability distribution of interfacial separations obtained for  $p = p_c$  (as given by the Persson contact mechanics theory). This approach ignores the increase in the surface separation observed when  $p_0$  decreases below  $p_c$  (see the dashed line in Fig. 23).

## Notes and references

- 1 D. J. Meyer, M. A. Peshkin and J. E. Colgate, World Haptics Conference (WHC), 2013, 2013, pp. 43–48.
- 2 C. Xu, A. Israr, I. Poupyrev, O. Bau and C. Harrison, CHI'11 Extended Abstracts on Human Factors in Computing Systems, 2011, pp. 317–322.

- 3 H. Tang and D. J. Beebe, *IEEE Transactions on Rehabilitation Engineering*, 1998, **6**, 241–248.
- 4 S.-C. Kim, A. Israr and I. Poupyrev, Proceedings of the 26th Annual ACM Symposium on User Interface Software and Technology, 2013, pp. 531–538.
- 5 D. Wijekoon, M. E. Cecchinato, E. Hoggan and J. Linjama, International Conference on Human Haptic Sensing and Touch Enabled Computer Applications, 2012, pp. 613–624.
- 6 M. Wiertelowski, R. F. Friesen and J. E. Colgate, *Proceedings of the National Academy of Sciences*, 2016, **113**, 9210–9215.
- 7 M. K. Saleem, C. Yilmaz and C. Basdogan, *IEEE Transactions on Haptics*, 2018.
- 8 A. Johnsen and K. Rahbek, *Journal of the Institution of Electrical Engineers*, 1923, **61**, 713–725.
- 9 E. Mallinckrodt, A. Hughes and W. Sleator Jr, *Science*, 1953.
- 10 T. Nakamura and A. Yamamoto, *ROBOMECH Journal*, 2017, **4**, 18.
- 11 J. Shintake, S. Rosset, B. Schubert, D. Floreano and H. Shea, *Advanced Materials*, 2016, **28**, 231–238.
- 12 G. Monkman, *Industrial Robot: An International Journal*, 2003, **30**, 326–330.
- 13 R. M. Strong and D. E. Troxel, *IEEE Transactions on Man-Machine Systems*, 1970, **11**, 72–79.
- 14 C. D. Shultz, M. A. Peshkin and J. E. Colgate, World Haptics Conference (WHC), 2015 IEEE, 2015, pp. 57–62.
- 15 S. Grimnes, *Acta Physiologica*, 1983, **118**, 19–25.
- 16 B. N. J. Persson, *Sliding Friction: Physical Principles and Applications*, Springer, Heidelberg, 2000.
- 17 E. Gnecco and E. Meyer, *Elements of Friction Theory and Nanotribology*, Cambridge University Press, 2015.
- 18 J. N. Israelachvili, *Intermolecular and Surface Forces*, Academic Press, 2011.
- 19 Y. Vardar, B. Güçlü and C. Basdogan, *IEEE Transactions on Haptics*, 2017, **10**, 488–499.
- 20 B. N. J. Persson, *The Journal of Chemical Physics*, 2018, **148**, 144701.
- 21 B. N. J. Persson, *Journal of Physics: Condensed Matter*, 2008, **20**, 315007.
- 22 B. N. J. Persson and M. Scaraggi, *The Journal of Chemical Physics*, 2014, **141**, 124701.
- 23 A. Almqvist, C. Campaná, N. Prodanov and B. N. J. Persson, *Journal of the Mechanics and Physics of Solids*, 2011, **59**, 2355–2369.
- 24 L. Afferrante, F. Bottiglione, C. Putignano, B. N. J. Persson and G. Carbone, *Tribology Letters*, 2018, **66**, 75.
- 25 B. N. J. Persson, *The Journal of Chemical Physics*, 2001, **115**, 3840–3861.
- 26 B. N. J. Persson, *Journal of Physics. Condensed matter : an Institute of Physics journal*, 2012, **24**, 095008.
- 27 A. Chateauminois and C. Fretigny, *The European Physical Journal E*, 2008, **27**, 221.
- 28 K. G. Rowe, A. I. Bennett, B. A. Krick and W. G. Sawyer, *Tribology International*, 2013, **62**, 208–214.

- 29 B. Lorenz, Y. Oh, S. K. Nam, S. H. Jeon and B. N. J. Persson, *The Journal of Chemical Physics*, 2015, **142**, 194701.
- 30 B. N. J. Persson, A. Kovalev and S. N. Gorb, *Tribology Letters*, 2013, **50**, 17–30.
- 31 A. E. Kovalev, K. Dening, B. N. J. Persson and S. N. Gorb, *Beilstein Journal of Nanotechnology*, 2014, **5**, 1341.
- 32 P. G. Whitten and H. R. Brown, *Physical Review E*, 2007, **76**, 026101.
- 33 T. Vodlak, Z. Vidrih, E. Vezzoli, B. Lemaire-Semail and D. Peric, *Biotribology*, 2016, **8**, 12–25.
- 34 T. Yamamoto and Y. Yamamoto, *Medical and Biological Engineering*, 1976, **14**, 494–500.
- 35 B. M. Dzidek, M. J. Adams, J. W. Andrews, Z. Zhang and S. A. Johnson, *Journal of The Royal Society Interface*, 2017, **14**, 20160935.
- 36 S. Bochereau, B. Dzidek, M. Adams and V. Hayward, *IEEE Transactions on Haptics*, 2017, **10**, 456–465.
- 37 H. Fruhstorfer, U. Abel, C.-D. Garthe and A. Knüttel, *Clinical Anatomy: The Official Journal of the American Association of Clinical Anatomists and the British Association of Clinical Anatomists*, 2000, **13**, 429–433.
- 38 S. Derler, L.-C. Gerhardt, A. Lenz, E. Bertaux and M. Hadad, *Tribology International*, 2009, **42**, 1565–1574.
- 39 Y. Yuan and R. Verma, *Colloids and Surfaces B: Biointerfaces*, 2006, **48**, 6–12.
- 40 C. Pailier-Mattei, S. Pavan, R. Vargiolu, F. Pirot, F. Falson and H. Zahouani, *Wear*, 2007, **263**, 1038–1043.
- 41 M. Geerligs, L. Van Breemen, G. Peters, P. Ackermans, F. Baaijens and C. Oomens, *Journal of Biomechanics*, 2011, **44**, 1176–1181.
- 42 M. J. Adams, B. J. Briscoe and S. A. Johnson, *Tribology Letters*, 2007, **26**, 239–253.
- 43 A. Tiwari, N. Miyashita, N. Espallargas and B. N. J. Persson, *The Journal of Chemical Physics*, 2018, **148**, 224701.
- 44 P. R. Gray, P. Hurst, R. G. Meyer and S. Lewis, *Analysis and Design of Analog Integrated Circuits*, Wiley, 2001.
- 45 C. Hsieh, H. Jain and E. Kamitsos, *Journal of Applied Physics*, 1996, **80**, 1704–1712.
- 46 D. Fischer, *Fujitsu Microelectronics Europe*, 2010.
- 47 Y. S. Papir, K.-H. Hsu and R. H. Wildnauer, *Biochimica et Biophysica Acta (BBA)-General Subjects*, 1975, **399**, 170–180.
- 48 X. Liu, *PhD thesis*, University of Sheffield, 2013.
- 49 M. Ayyildiz, M. Scaraggi, O. Sirin, C. Basdogan and B. N. J. Persson, *Proceedings of the National Academy of Sciences*, 2018.
- 50 B. Delhayé, P. Lefevre and J.-L. Thonnard, *Journal of The Royal Society Interface*, 2014, **11**, 20140698.
- 51 C. Shultz, E. Colgate and M. A. Peshkin, *IEEE Transactions on Haptics*, 2018, **11**, 279–290.
- 52 R. Oftadeh, B. K. Connizzo, H. T. Nia, C. Ortiz and A. J. Grodzinsky, *Acta Biomaterialia*, 2018, **70**, 249–259.
- 53 L. Pastewka, N. Prodanov, B. Lorenz, M. H. Müser, M. O. Robbins and B. N. J. Persson, *Physical Review E*, 2013, **87**, 062809.
- 54 S. Derler and L.-C. Gerhardt, *Tribology Letters*, 2012, **45**, 1–27.
- 55 C. Hendriks and S. Franklin, *Tribology Letters*, 2010, **37**, 361–373.
- 56 S. Tomlinson, R. Lewis and M. Carré, *Wear*, 2009, **267**, 1311–1318.
- 57 H. P. Saal, B. P. Delhayé, B. C. Rayhaun and S. J. Bensmaia, *Proceedings of the National Academy of Sciences*, 2017, **114**, E5693–E5702.
- 58 B. N. J. Persson, *The European Physical Journal E*, 2002, **8**, 385–401.
- 59 F. W. Strong, J. L. Skinner, P. M. Dentinger and N. C. Tien, *Reliability, Packaging, Testing, and Characterization of MEMS/MOEMS V*, 2006, p. 611103.
- 60 T. André, V. Lévesque, V. Hayward, P. Lefèvre and J.-L. Thonnard, *Journal of The Royal Society Interface*, 2011, **8**, 1574–1583.
- 61 B. N. J. Persson, B. Lorenz and A. Volokitin, *The European Physical Journal E*, 2010, **31**, 3–24.
- 62 B. N. J. Persson, *Tribology Letters*, 2016, **63**, 42.